Engineering Structures 318 (2024) 118689

Contents lists available at ScienceDirect

Engineering Structures

journal homepage: www.elsevier.com/locate/engstruct

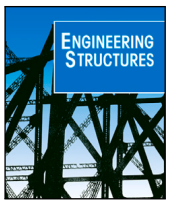

A new hold-down device for seismic applications in CLT buildings: Design, testing, analytical and numerical assessment

A. Marchisella *, G. Muciaccia

Department of Civil and Environmental Engineering, Politecnico di Milano, Milano, Italy

ARTICLE INFO

Keywords:
Hold-down
Seismic
Anchors
CLT
2G Eurocodes

ABSTRACT

An hold-down device was designed and tested experimentally for seismic applications (Seismic Hold-Down, SHD). The magnitude of axial strength as well as the up-lift displacement capacity is mainly oriented to cross-laminated-timber (CLT) buildings with medium-to-high ductility. There is consensus in the design practice of hold-down devices for promoting, as dissipative mechanism, flexural yielding of the dowel-type connectors (e.g. nails, screws) combined to timber's embedment. Few are the applications aiming at hold-down's optimization as it emerges from up-to-date literature review. In this framework, SHD was conceived such that tension break-out of steel was promoted at a reduced segment (fuse) of the vertical flange. In the context of capacity design, a convenient overstrength was assumed for other failure mechanisms, e.g. anchor's pullout, laterally-loaded steel-to-timber connection, shear-plug of timber. The mechanical response under axial load was consistently predicted by an application of the component method, i.e. global stiffness and strength were analytically-derived using simplified series of non-linear mechanical springs. Three-dimensional finite elements model was employed to investigate buckling of the fuse which might occur, during cycles, when up-lift displacement is recovering. In practical circumstances, it is recommend to design SHD devices of a CLT wall similarly to diagonal elements of steel bracings, i.e. neglecting the contribution of the compressed element. Finally, SHD is compared to traditionally-designed hold-down, which mostly dissipates (and fails) at steel-to-timber connection. Overall hysteretic response is somehow similar, although the inelastic mechanisms involved are different. For example, both the devices show pinching during cycles which for SHD is mainly caused by buckling of the fuse while, for traditional hold-down, is dominated by timber's embedment.

1. Introduction

There is an on-going popularity of timber buildings mainly sponsored by sustainability arguments, e.g. reduction of carbon-dioxide emission and fossil fuel consumption [1]. Furthermore, consensus is growing about satisfactorily buildings' performance against earthquake if compared to both reinforced concrete and steel [2].

Generally, for timber buildings the seismic-resistant structural elements are shear walls [3] which may consist of either a single or multiple cross-laminated-timber (CLT) panels [4]. Connection to concrete foundation is usually made using metal connectors (hold-down, angle brackets) which are nailed at timber side and anchored at concrete side. According to [5], a single panel shear wall generally leads to medium ductility (DC2) whereas high ductility could be reached only using multiple panels connected by vertical joints (DC3). For example, suggested behavior factors (q) are 2.3 and 3.2 for DC2 and DC3, respectively. Yet, for dissipative zones such as hold-down connections a minimum value is required for ductility, i.e. $\mu = d_u/d_y > 1.5$ where d_u and d_y are ultimate and yielding displacements, respectively.

Rocking response of a single-storey CLT shear wall is shown in Fig. 1a. Foundations blocks are not used as sources of hysteretic energy dissipation [6], therefore they are designed to remain elastic under the design seismic action. Indeed, the foundation block is supposed neither to slide nor to rotate or to mobilize the bearing-capacity failure mechanism of soil. Evidences which suggest that soil–structure interaction (SSI) is significant for CLT buildings are few if compared to other structural types (e.g. reinforced concrete [7]) although the influence of super-structure on SSI is known to be minor [8]. To the Authors' knowledge, one study [9,10] considered SSI for CLT buildings (1 and 3 storey) tested within SOFIE project [11]. Results of linear time-histories analyses show that peak displacement demand increased as decreasing shear wave velocity, e.g. from 325 to 150 m/s being the latter characterizing soft-soil condition. Generally, CLT structures may reach structure-to-soil stiffness ratio ($\frac{1}{\sigma} = \frac{h}{V_s \cdot T}$, where h is the building height, V_s is the shear wave velocity, and T is the fixed-end natural period) larger than 0.1 which has been given as threshold for

* Corresponding author.
E-mail address: angelo.marchisella@polimi.it (A. Marchisella).

https://doi.org/10.1016/j.engstruct.2024.118689
Received 20 March 2024; Received in revised form 10 July 2024; Accepted 24 July 2024
Available online 7 August 2024

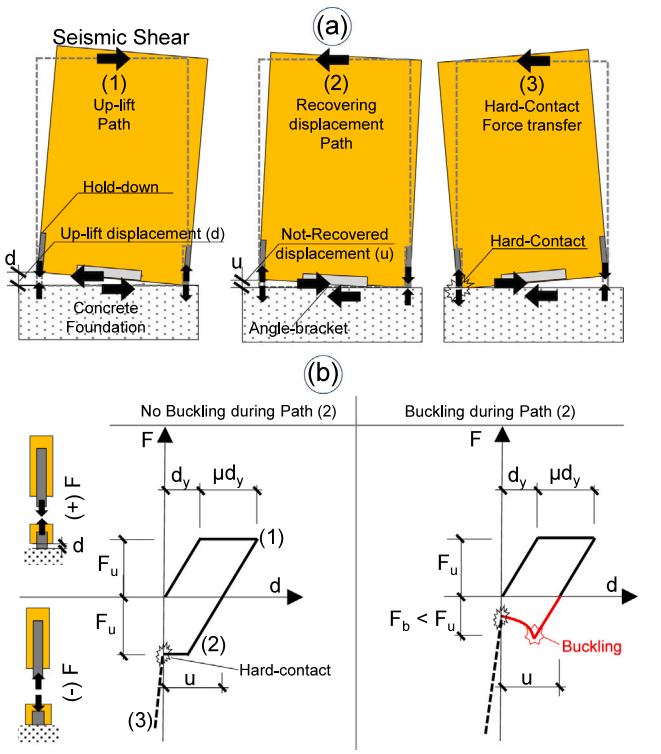

Fig. 1. Single-story timber shear panel (e.g. CLT) connected to concrete foundation using hold-down and angle brackets connections: (a) fundamentals of rocking mechanism; (b) load-to-displacement curve for hold-down. (Notes. Displacements were exaggerated for representation purposes. Both sliding displacements and membrane deformation of the panel are not shown. For the sake of simplicity, point of hard-contact is assumed at the panel's edge. The Reader is referred to the color version of this figure.)

the neglection of SSI [8], but as a matter of facts routine structural analysis of CLT buildings [12–14], as well as design codes [5], do not consider soil's deformability either in elastic or non-elastic regime.

As per the super-structure, i.e. CLT wall, hold-down connections are prevalently loaded axially (in tension) due to overturning moment. Compressive forces are directly transferred via hard-contact between the wall and concrete foundation. Sliding of the wall is restrained primarily by angle brackets. Friction, activated by vertical compression acting on the wall, may contribute to restraint sliding [15], although it is generally neglected in design practice [16] especially because experimental evidences of cyclic response are contradictory [17]. Rocking of the CLT wall is dominant with respect to both membrane deformation of and sliding, e.g. contribution to lateral drift could be up to 80% [17].

Typical mechanical responses of hold-down isolated from cyclically-loaded shear wall, are represented in Fig. 1.b. For the sake of simplicity, only one load cycle is shown. Up-lift displacement (d) and associated tensile force (F) are assumed as positive. In up-lift direction the behavior may be conveniently represented as elastic–plastic characterized by strength equal to F_u, yield displacement d_y and up-lift level equal to $\mu \cdot d_y$. When up-lift displacement is recovered ($d = 0$), compression is expected to be transferred via hard-contact between wall and foundation. However, during displacement recovering ($0 < d < u$) buckling of the vertical flange might occur at a load level (F_b) lower than F_u.

Fig. 2.(a)-to-(d) shows typical failure mechanisms, in tension, experimentally observed for hold-down connections such as break-out of the vertical flange, anchorage's failure, yielding of laterally-loaded screws, plug shear. Buckling of the compressed vertical flange has been observed as well, e.g. Fig. 2.e. In practical design circumstances, steel-to-timber connection is promoted as ductile link, providing that the connectors (e.g. screws or nails) develop one or two plastic hinges. Other possible failure mechanisms (e.g. anchorage failure, breaking of the metal flange) should be over-strong. For example, reference overstrength factors (γ_{Rd}) according to European practice are: (i) γ_{Rd} = 1.6 according to [5] which background was given in [18,19]; (ii) γ_{Rd} = 1.3, frequently suggested in absence of further specifications from [20], e.g. [14,21,22].

Experimental characterization of hold-down connections is usually made at a reduced scale (sub-assemblage) with respect to the panel, e.g. [22–24]. Axial-only load condition is commonly assumed consistently with respect to design methods [15]. In fact, according to experimental observations [22], typical hold-downs exhibits relatively high strength and stiffness capacity in tension, while in shear direction strength and stiffness are significantly reduced due to local buckling. Coupled axial-to-shear response has been further investigated [25,26] showing that coexistent shear force decreased the tension capacity, e.g. for lateral displacement larger than 7.5 mm the force decrease at peak can be up to 25%. When yielding of the connectors is achieved in uniaxial tension, the experimentally-derived axial bearing capacity is generally [23] comparable to analytical prediction using European Yield Model [27]. Such failure mechanism lead to moderate-to-high ductility, e.g. μ = 2.7÷4.3 [24], 2.8 [22]. Stiffness predicted according to [28], accounting only for slip between timber and connectors (e.g. nails), results significantly larger than experimental values, e.g. up to five times. Such discrepancy is mainly due to neglection of displacement contributions such as the one of the anchor as well as elongation of steel plate.

Anchorage-to-concrete has been recognized as one of the most challenging issue to solve in hold-down connection because up-lift forces might be not comparable in magnitude with respect to concrete-related strengths of anchors, if they are supposed to be installed in cracked concrete under so called "seismic conditions". For example, to fulfill overstrength requirements, steel beams are embedded in concrete foundation [12,29–31]. However, the anchorage problem is somehow neglected in experimental characterizations. In fact, when tested, hold-down devices are frequently fixed to steel beams rigidly connected to reaction floor. Although such assumption is made to promote a specific failure mechanism (e.g. shear failure of dowel-type connectors) anchor's displacement in concrete may be not negligible, notwithstanding the assumed overstrength.

As mentioned before, design practice of CLT buildings is mainly oriented to traditional hold-down devices(promoting failure at steel-to-timber connection), nevertheless there have been attempts for optimization. For example, in [32] a fuse is introduced at the base plate of hold-down device such that the failure is shifted from steel-to-timber connection to a T-stub [33] portion. In such a case, the cyclic behavior show stable response, with low degradation of stiffness, strength, and energy dissipation. Similar promotion of steel hysteretic behavior is assumed for the x-shaped hold-down proposed in [34–36], although in this case buckling occurred for high ductility demand, e.g. axial displacement larger than 30 mm. Finally, within the context of optimized hold-down, re-centering hold-down devices proposed in [37,38] should be mentioned albeit, to the Authors' opinion, their foreseeable high cost may limit their applicability in practical circumstances.

This paper characterizes an hold-down device designed to promote steel failure in a portion of the steel flange, which was intentionally reduced in area (termed "fuse" throughout the paper). As per the conception of the device, affinities are recognized with respect to [32]. However, the resulting mechanical response shows much more similarities with respect to [36] due to buckling occurrence. The paper is structured as it follows. In Section 2, capacity design of the hold-down is presented along with experimental characterization under static and cyclic loads (some of the contents of this section were presented by the Authors in a conference paper [39]). Expanded version of calculations for analytically-assessed failure mechanisms as well as for structural analysis are given in Appendices A and C, respectively.

In Section 3, experimental results are discussed with respect to both analytically (additionally detailed in Appendix B) and numerically-derived predictions of hold-down's mechanical response.

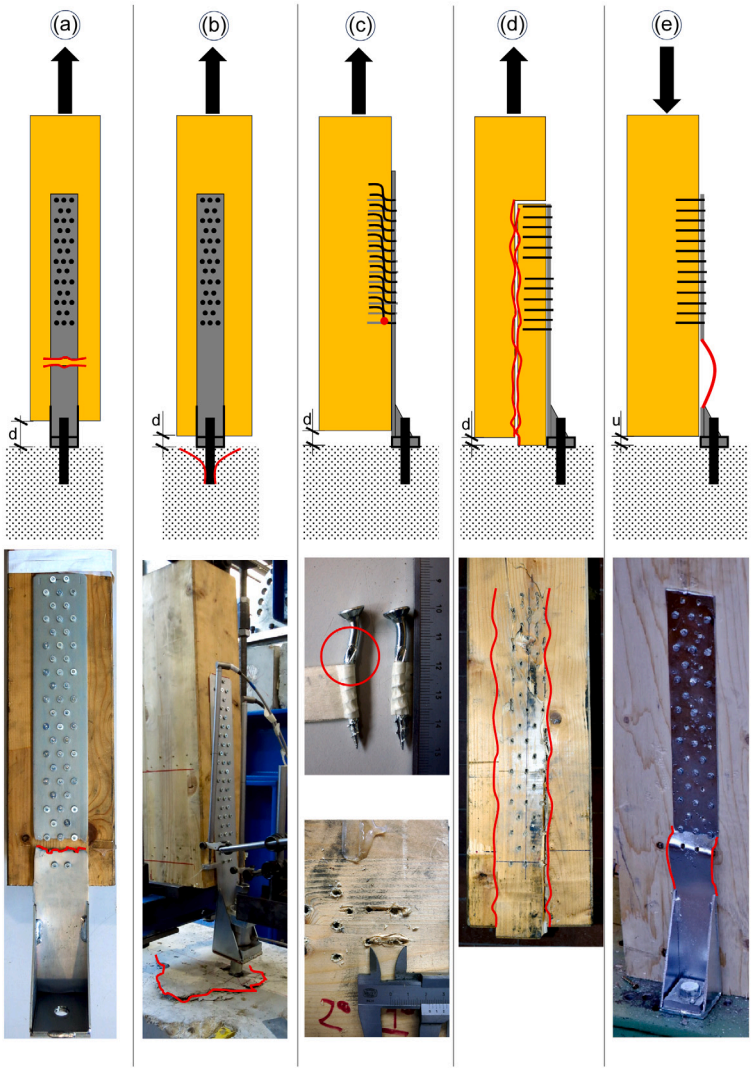

Fig. 2. Typical failure modes for hold-down connection: (a) steel break-out in tension; (b) anchorage's failure; (c) plastic hinge of screws combined to embedment of timber; (d) plug-shear; (e) buckling of steel flange. (Notes. Photographic evidences (a)-to-(d) were partly adapted either from [39] or unpublished material available to the Authors. Photo (e) was adapted from [22], courtesy of Massimo Fragiacomo. The Reader is referred to the color version of this figure.)

In Section 4 conclusions and design recommendations are given.

The Authors have privileged, throughout the paper, references to Second Generation Eurocodes [40] although the drafts they consulted, accessed at https://bsol.bsigroup.com/ in September 2023, may suffer changes.

2. Experimental program

2.1. Capacity design of SHD

Three hold-down devices were designed and tested experimentally as dissipative connections for seismic application (succinctly termed Seismic-Hold-Downs, SHD, throughout the paper). Failure of the steel vertical flange was promoted by introducing a fuse zone (with extension l_f, occasionally termed "stretch length"), i.e. a portion of the flange with reduced area. Details of the geometries as well as material characteristics are given in Table 1. The axial bearing capacities (design values) resulting from steel break-out of the fuse are equal to 39/22/14 kN for SHD-620/540/440, respectively. The increase of strength according to the height results from the increase (i) of fuse's area and (ii) the number of the connectors. Such alternatives axial capacities are intended to cover wide range of applications in practical design of CLT buildings. In fact, it may be economically convenient to design the hold-down connection without excessive margin with respect to the seismic demand. Generally, the magnitude of the strengths as well as the displacement capacities are such that SHD are oriented to applications for medium-to-high ductility CLT buildings, e.g. case study proposed in [13].

Within the framework of capacity design approach, γ_{Rd} factors were analytically-derived for failure modes shown in Fig. 2. For space limitation, all the calculations are given in Appendix A. A brief description of the background assumptions for structural analysis as well as strengths' evaluation is given hereinafter.

- *Structural Analysis*
  SHD devices were designed (and tested) to resist only tension force. Fig. 3.a shows the assumed configuration, i.e. two SHD are installed at the corner of a CLT wall. Vertical force due to overturning ($2F$) is symmetrically-distributed such that each SHD is loaded by F. Further, due to eccentricity ($b/2$) between the force F and the anchor's force (F_a), a parasitical bending moment need to be transferred to foundation. If the base plate rotates rigidly (Fig. 3.b) its deformed shape can be approximated to rigid rotation around the toe. Regardless the magnitude of displacements, F_a can be derived as it follows according to rotational

Table 1
Hold-down devices designed for seismic application (SHD).

SHD	620	540	440		Description/Formulas
Geometry according to [41]					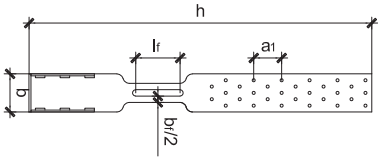
h	620	540	440	(mm)	
b	80	70	60	(mm)	
t	3	3	2.5	(mm)	
l_f	50	70	70	(mm)	
b_f	45	25	20	(mm)	
Steel material parameters					
	S235JR[a]	S235JR[b]	S235JR	(–)	Steel class according to [42]
f_{yk}	235	235	235	(MPa)	Characteristic yield stress
f_{uk}	360	360	360	(MPa)	Characteristic ultimate stress
E	200 000	200 000	200 000	(MPa)	Young modulus
Screws					
n_{tot}	45	30	20	(–)	Number of screws
d	5	5	5	(mm)	Diameter
t_{pen}	40	40	40	(mm)	Penetration depth
a_1	44	44	44	(mm)	Parallel to grain spacing
Anchors					
Type	BO	SL	SL	(–)	BO—Bonded anchor; SL—Sleeve anchor
d	20	24	20	(mm)	Anchors' diameter
h_{eff}	350	150	100	(mm)	Embedment depth
Timber post					
	GL24h			(–)	Timber glulam class according to [43]
Concrete foundation					
	C20/25			(–)	Concrete class according to [44]
Experimental tests					
Static	1	1	1	(–)	According to [45]
Cyclic	1	1	1	(–)	

[a] S355JR was used for both static and cyclic experimental characterization.
[b] S355JR was used for cyclic experimental characterization.

equilibrium around the toe of the base plate:

$$F_a \cdot b/2 = F \cdot b - \cancel{(M_f - V_f \cdot h_{st})} \qquad F_a = 2 \cdot F \tag{1}$$

where $M_f - V_f \cdot h_{st}$ is the contribution due to bending of the vertical flange outside the stiffened portion (h_{st}) which, for the sake of simplicity, is neglected. In fact, M_f (and consequently V_f) can reach values up to the plastic moment of the flange which is considerably lower with respect to $F \cdot b$. On this subject, further details can be found in Appendix C where a numerical example is given considering both all terms in Eq. (1) and displacements' compatibility. Usually, technical specifications of hold-down devices refer to the eccentricity ratio (k_t) evaluated as it follows:

$$k_t = \frac{F_a}{F} = 2.0 \tag{2}$$

Alternatively [46], $k_t = 2.5$ was derived taking into consideration that compression point moves towards the anchor as shown in Fig. 3.c. Generally, the effect of anchor's preload (P) is not considered when evaluating k_t. In fact, for $F_a < P$ rotation of the base plate is prevented. As a result, k_t should be assumed equal to 1.0. Nevertheless, $F_a > P$ is commonly assumed at ultimate limit state.
In designing SHD, k_t has been assumed equal to 2.0. A further discussion based on experimentally-derived k_t is given in Section 2.3.

- *Steel tension break-out*
  Ultimate design strength ($N_{Rd,s}$) is evaluated as the product between the fuse's area (A_f) and ultimate design strength (f_{ud}). Partial factor for material for the case of resistance of metal plate in steel-to-timber connections was assumed according to [47].
- *Buckling*
  Euler's buckling load ($N_{b,Rd}$) is evaluated as $N_{b,Rd} = \pi^2 \frac{E \cdot J}{l_0^2 \cdot \gamma_{M1}}$ where EJ is the fuse's flexural modulus along the weak axis, l_0 is assumed equal to the stretch length, partial factor (γ_{M1}) for steel material under buckling case was assumed according to [48]. Analytically-derived overstrength ratio is evaluated as $\gamma_{Rd} = \frac{N_{b,Rd}}{N_{Rd,s}}$. Essentially, buckling is supposed to occur within the stretch length (behaving as a beam) being the remaining portions of the vertical flange effectively restrained. Such assumption has been further supported by numerical study presented in Section 3.2.
- *Laterally-loaded screws*
  Lateral-load capacity ($F_{vrd,tot}$) is evaluated according to European Yield Model [27] as the product between the total number of screws (n_{tot}) and the design resistance of single connector (F_{vrd}). Analytically-derived overstrength ratio is evaluated as $\gamma_{Rd} = \frac{F_{vrd,tot}}{N_{Rd,s}}$. For the sake of completeness, resistance has been evaluated applying reduction factor ($\Psi_{eff} = n_{eff}/n_{tot} < 1.0$) which considers the effective numbers of screws parallel to grain (n_{eff}) although the Authors believe that conditions stated in [49] corroborated by experimental evidences in [50] apply. Indeed, in respect of laterally-loaded connections composed by dowel-type fasteners in CLT, the ductile behavior in case of side face insertion, which is due to the orthogonal reinforcing layup of CLT, enables $n_{tot} = n_{eff}$. Although the application of SHD is mainly oriented to CLT, experimental characterization, presented in the following, adopted glulam for practical convenience. In this regard, it should be noticed that according to [49], fasteners inserted via the CLT side face (as the ones of SHD) can be designed similarly to fasteners in solid timber and glulam. Yet, fasteners inserted via the CLT side face and loaded laterally show larger ductility with respect to glulam. Furthermore, it should be mentioned that according to [5], glulam panels may be used as an alternative to CLT although such circumstance is limited to low-ductility classes.
- *Plug-shear*
  Shear strength ($F_{v,la,d}$) of timber element was evaluated according to [47]. Nominal shear strength (f_{vk}) of glulam was obtained from [43]. Partial factor for material was according to [47]. Analytically-derived overstrength ratio is evaluated as $\gamma_{Rd} = \frac{F_{v,la,d}}{N_{Rd,s}}$.
- *Anchorage-to-Concrete*

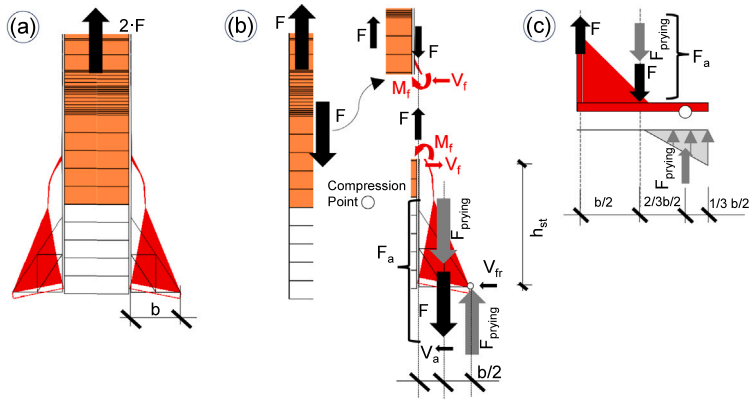

Fig. 3. Simplified mechanical model to analytically-derive anchor's force (F_a) and eccentricity coefficient (k_t) according to Eq. (2): (a) up-lift deformed double-side hold-down specimen; free-body diagrams (b) proposed by the Authors and (c) adapted form [46]. (Notes. Displacements were exaggerated for representation purposes.)

Axial strengths of anchors ($N_{Rd,a}$) were analytically-derived according to [51] considering single anchor far from edges. Although such condition might not be practical, it was representative for the adopted experimental setup. Post-installed anchor were used, i.e. bonded anchors (BO) and sleeve anchors (SL). Analytically-derived overstrength ratio is evaluated as $\gamma_{Rd} = \frac{N_{Rd,a}}{k_t \cdot N_{Rd,s}}$ where k_t was tentatively assumed equal to 2, according to Eq. (2). The resulting failure mechanisms were combined pullout-and-concrete cone for BO, and concrete cone for SL. Product-dependent parameters were derived from technical documents [52,53]. Seismic resistances were evaluated consistently with the criteria of Annex G of [54]. Seismic category C1 according to Annex C of [51] is assumed, instead of C2 which is prescribed for buildings when peak-ground-acceleration is larger than 0.05 g. According to definitions summarized in [55], C1 assessment procedure for post-installed anchors encompasses, among other tests, pulsating axial load test in cracked concrete. As per C2, anchors are tested in crack cycles. Because concrete foundations are normally capacity-designed to stay elastic beyond yielding [56], the need of C2 category for anchors is generally over-conservative.

The analytically-derived γ_{Rd} with respect to steel tension break-out in the fuse are reported in Table 2 along with reference values. Sufficient margin of overstrength is obtained for laterally-loaded screws and plug-shear if compared to reference values.

No overstrength is obtained for buckling of the fuse which might occur when recovering large up-lift displacements. This outcome implies that, within the framework of capacity design, SHD shall be considered as "tension-only" members similarly to diagonal elements of steel concentric bracings. In such a case, according to [5], the compressed diagonals may be neglected in the seismic analysis (e.g. equivalent static, modal-response-spectrum) providing that the resistance of the building in pre-buckling range of compressed diagonal members is smaller than the lateral resistance of the building evaluated with only the tension diagonals at yield. In the same way, for a CLT wall under rocking, SHD in compression shall be neglected providing that overturning strength in pre-buckling range is lower than the one evaluated with only the tensioned SHD at yielding.

For all SHD devices, anchorage-to-concrete is critical. In fact, using design values of strengths γ_{Rd} is either equal or lower than one for BO and SL, respectively. For practical circumstances it would have been sufficient to use, for all SHD, BO with increased embedment depth. Nevertheless to the scope of designing the specimens to be tested experimentally, γ_{rd} were evaluated using characteristic values of strengths. Such assumption, generally introduced in [18] for the design of ductile parts in timber structures, represents a compromise between either using mean or design values of strengths. For example, considering γ_{rd} between anchorage failure and steel break-out of the fuse, overstrength equation with characteristic values of strengths can be written as it follows:

$$\gamma_{rd} N_{Rk,s} = \gamma_{sc} \gamma_{an} N_{Rk,s} < \frac{N_{Rk,a}}{k_t} \tag{3}$$

where $\gamma_{sc} = \frac{N_{0.95,s}}{N_{0.05,s}}$ accounts for the scatter of strength distribution as the ratio between 95th ($N_{0.95,s}$) and 5th ($N_{0.05,s}$) percentile; $\gamma_{an} = \frac{N_{0.05,s}}{N_{Rk,s}}$ accounts for approximation in analytical model used to predict the strength. If both $\gamma_{an} = 1$ and normal probability density is applied to steel break-out of the fuse, γ_{rd} can be written as it follows:

$$\gamma_{rd} = \frac{1 + k_n COV}{1 - k_n COV} \approx 1.22 \tag{4}$$

where $k_n = 1.64$ and $COV = 0.06$ were assumed consistently with respect to [57]. Analytically-derived γ_{rd}, considering characteristic values of strengths, were larger than 1.2 with one exception, i.e. anchorage failure of SHD-440. Such outcome, as it is presented in the following, was investigated further by defining explicitly the probability density of the anchorage's strength based on experimental characterization.

To further demonstrate the sufficient overstrength between $N_{Rk,s}$ and $N_{Rk,a}$ the latter was directly derived from experimental characterization considering C1 seismic category for anchors [55]. Assuming that normal distribution applies to the observed maximum residual pullout forces (evaluated after pulsating load tests), both probability density and cumulative distribution were compared to the ones associated to steel break-out of the fuse. Comparison is shown in Fig. 4. In the light of overstrength concept, it is worth to mention that there is no region in the cumulative probability charts where the anchor's resistances are lower than the ones associated to break-out of steel fuses.

2.2. Test setup

Hold-down sub-assemblages were tested by adopting the setup shown in Figs. 5 and 6.a. Hold-down devices were symmetrically installed as connecting elements between a concrete foundation having concrete class C20/25 according to [44] and a timber (glulam) post having strength class GL24 h according to [43]. Such double configuration was adopted to eliminate out-of-plane displacements otherwise unavoidable due to eccentricity between load and anchor's reaction. The load was applied at center of the timber post using an hydraulic cylinder of 300 kN capacity. Timber post slides vertically, i.e. lateral displacements were restrained. Tests were displacement-controlled, i.e. the stroke of hydraulic actuator (which is generally termed as "cross-head displacement" throughout the paper) was set as a control variable applying a rate of 0.08 mm/s both for monotonic and cyclic tests. Local displacements were measured using linear-variable-differential-transformers (LVDTs), e.g. Fig. 6.b shows LVDTs at timber

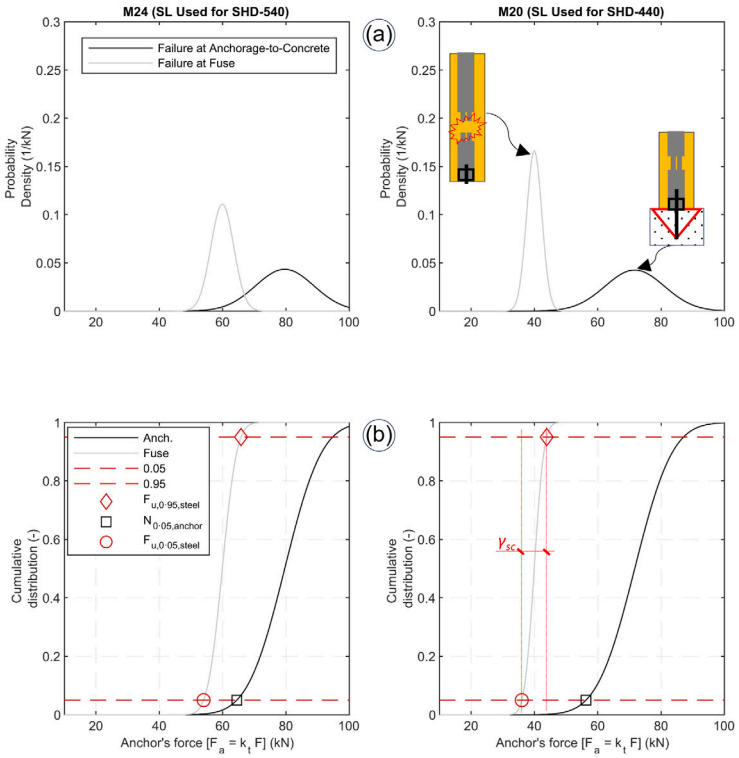

Fig. 4. Analytically-derived (a) probability densities and (b) cumulative distributions for relevant mode of failure characterizing SHD-540 and SHD-440. (Notes. γ_{sc} according to Eq. (4).)

Table 2
Analytically-derived overstrength factors (γ_{Rd}) with respect to steel failure at fuse for SHD devices.

Failure mode	ToF[a]	Ref.[b]	SHD		
			620	540	440
Using design values for strength					
Anchorage-to-concrete (single)	B	1.6(1.3)	1.0	0.9	0.7
Laterally-loaded screws	D	1.2(1.3)	1.7	2.1	2.1
Buckling	B	1.6(1.3)	0.8	0.6	0.4
Plug-Shear	B	1.6(1.3)	2.3	2.8	2.8
Using characteristic values for strength					
Anchorage-to-concrete (single)	B	1.2[c]	1.3	1.2	1.0
Laterally-loaded screws	D	1.2[c]	1.8	2.1	2.1
Buckling	B	1.2[c]	0.8	0.6	0.4
Plug-Shear	B	1.2[c]	2.9	3.5	3.6

[a] Type of failure: (B) brittle and (D) ductile.
[b] Overstrength factor according to [5] and () to [21].
[c] Intentionally assumed by the Authors for experimental characterization.

post and steel flange. Anchors' forces were monitored using washer load cells (compression-only) as the one shown in Fig. 6.c.

For cyclic tests, displacement protocol according to [45] was adopted with the following specifications:

- SHD were not designed to promote failure in steel-to-timber connection, thus the cross-head displacement was assumed as relevant kinematic variable instead of slip between steel plate and timber post as it would be if [45] was applied rigorously. Such assumption was encouraged by specifications of [58] where kinematic variables are generally referred as "displacements".
- Displacement protocol is shown in Fig. 7. Cycles are referred as "push-zero", i.e. displacements are not inverted in sign. Such assumption is generally coherent with respect to the expected displacement history at the corner of a CLT wall under seismic conditions.
- Target up-lift displacements (d) are multiples of the nominal yielding displacement (d_y) defined in preliminary static tests, i.e. d = 0.75–1.00–1.5–2.00·V_y-etc... up to failure. Each cycle is repeated three times to evaluate possible impairment of strength. Displacements are generally limited to 30 mm.

2.3. Experimental results

Results of experimental tests are shown in Fig. 8.a/b/c for SHD-440/540/620, respectively. The experimental load-to-displacement curves are shown along with analytically-derived ones, although the latter are discussed in Section 3.1.

All the specimens showed similar failure sequence as the one represented in Fig. 9.a/b/c. For displacements larger than 20 mm, the fuse underwent discernible necking phenomena before breaking. Residual slip between steel plate and timber was non significant. Besides, concrete foundation was undamaged. Only one side failed in all tests, i.e. west or east. Such evidence might be attributed either to non-intentional eccentricities which, affected the test setup despite all effort, or non-symmetrical material characteristics.

Cyclic behavior was characterized by envelope curves similar to the static ones without strength reduction. Such result generally confirms that the dominant plastic mechanism was the elongation of steel fuse without significant degradation of steel-to-timber connection. In fact in such a case, a 20% reduction of strength would have been expected [21]. Furthermore, non-significant impairment of strength were observed between consecutive cycles.

Fig. 10 shows experimentally-derived eccentricity ratios (k_t, according to Eq. (2)) for static tests. Generally, when F is larger than the anchor's preload, k_t is larger than one. Additionally, k_t is maximum at yielding while it reduces approaching ultimate load. Comparison between experimentally-derived k_t (assumed, for simplicity, at yielding) and analytical predictions is given in Table 3. It is worth to mention that, experimental k_t are lower than 2.0 which was tentatively assumed

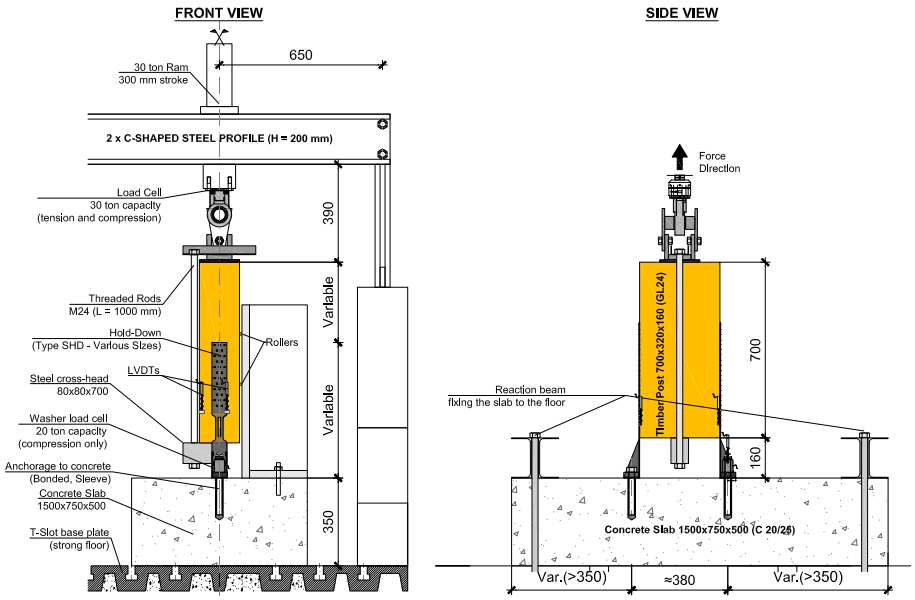

Fig. 5. Experimental setup used to test SHD statically and cyclically. (Notes. The Reader is referred to the color version of this figure.)

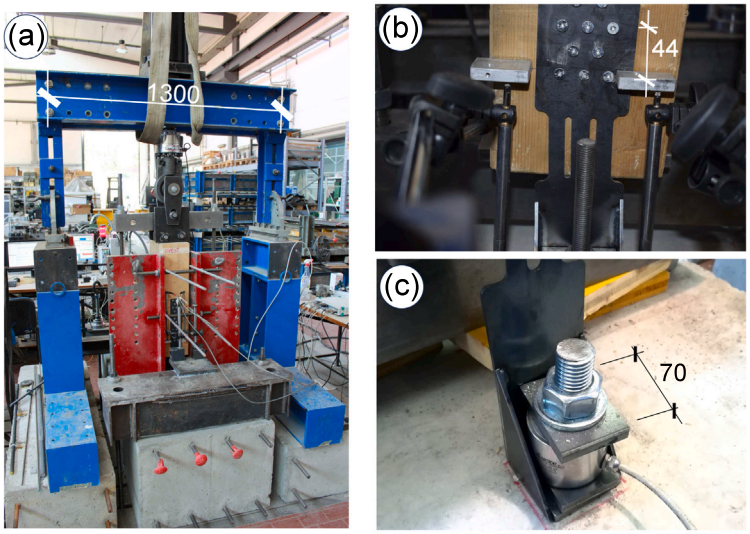

Fig. 6. Experimental setup used to test SHD statically and cyclically, photographs: (a) setup's layout; (b) displacements measurements; (c) washer load cell. (Notes. Dimensions are given in millimeters. The Reader is referred to the color version of this figure.)

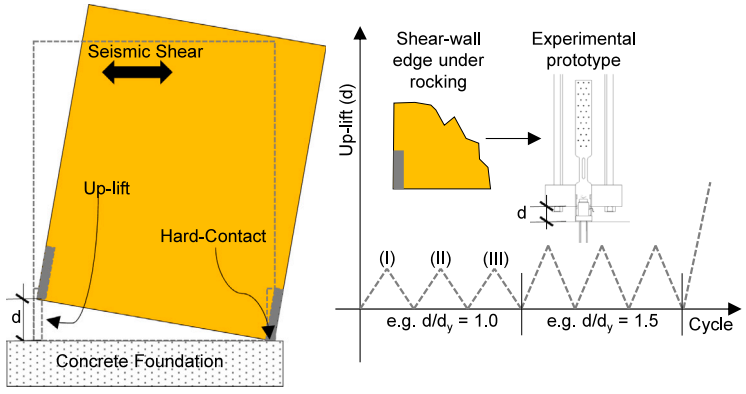

Fig. 7. Applied cyclic displacement protocol, for SHD, according to [45]. (Notes. Displacements were exaggerated for representation purposes.)

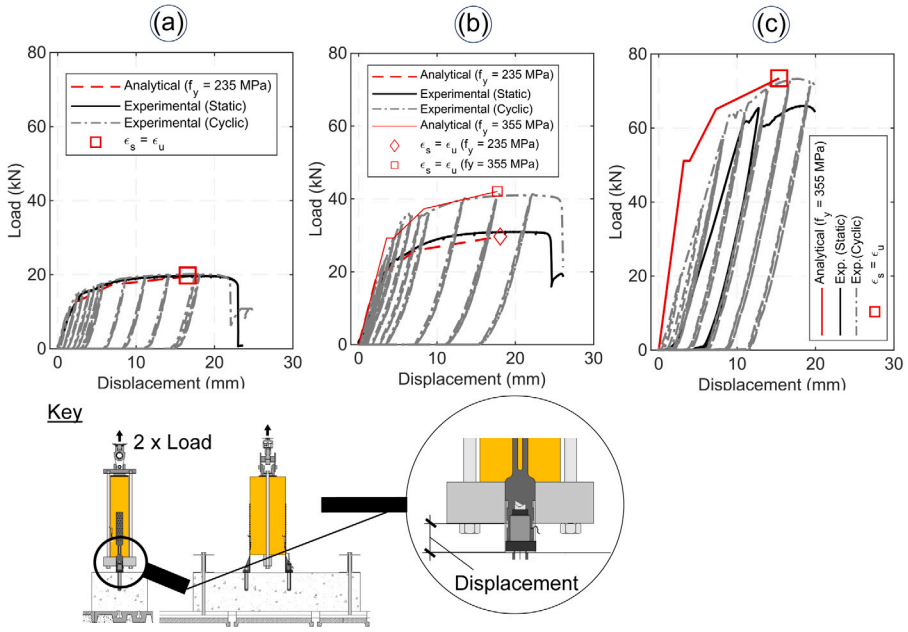

Fig. 8. Experimental results for SHD: (a) SHD–440; (b) SHD–540; (c) SHD-620. (Notes. The Reader is referred to the color version of this figure.)

Table 3
Experimentally-derived anchors' forces and eccentricity coefficients (k_t) for static (St.) and cyclic (Cy.) tests.

SHD		440[a]		540		620	
		St.	Cy.	St.	Cy.	St.	Cy.
$F_{a,west}$	(kN)	–	–	42.6	35.9	101.5	–
$k_{t,west}$	(–)			1.8	1.6	1.6	
$F_{a,east}$	(kN)	–	–	38.1	47.4	124.1	–
$k_{t,east}$	(–)			1.6	2.1	1.9	
F	(kN)	–	–	24.0	22.8	65.3	–
$k_{t,anal}$[b]	(–)				2.0/2.5		
$k_{t,num}$[c]	(–)				1.9		

[a] Anchors' forces not monitored.
[b] Analytically-derived eccentricity coefficient ($k_{t,anal}$) according to Eq. (2) and [46].
[c] Numerically-derived eccentricity coefficient ($k_{t,num}$) based on numerical model for SHD-540 presented in 3.2.

in design phase. For practical design circumstances, when overstrength is evaluated at steel break-out, values lower than 1.5 can be assumed.

Finally, a non-perfect displacement recover was observed in cyclic tests. Although the cross-head displacement was forced to reach zero value in unloading path, displacement measured at timber post and steel flange were not recovered. Such results was caused by unexpected lack of contact during unloading between connecting elements of the actuator and cross-head. Simply put, kinematic constraint between cross-head and timber post revealed to be mono-lateral in such a way that, for large up-lift displacements, a gap formed when unloading therefore zero reaction was observed. Under this circumstance, the experimental assessment of mechanical behavior was considered partial and a further investigation with emphasis on the unloading paths was carried out using numerical models as it is presented in Section 3.2.

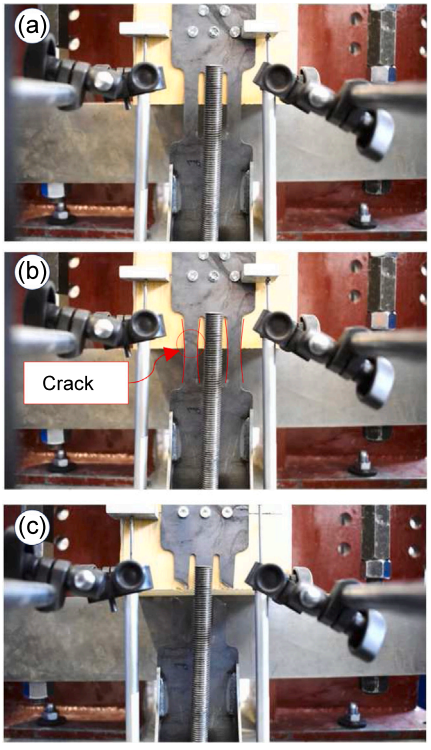

Fig. 9. Typical failure sequence of the fuse for SHD: (a) undeformed; (b) necking and cracking; (c) breaking. (Notes. Photographs refer to SHD-620 tested statically. The Reader is referred to the color version of this figure.)

3. Discussion

3.1. Simplified analytical model

Fig. 11 shows a simplified analytical model (series of springs) which has been adopted to predict load-carrying capacities as well as displacements for SHD. The model was inspired by "Components' Method" [59], developed for steel connections. Nonetheless, a similar series of springs was adopted in [22] to discuss results of traditionally-designed hold-down, i.e. designed such that the weakest spring was the steel-to-timber connection. In that case, controversial results were

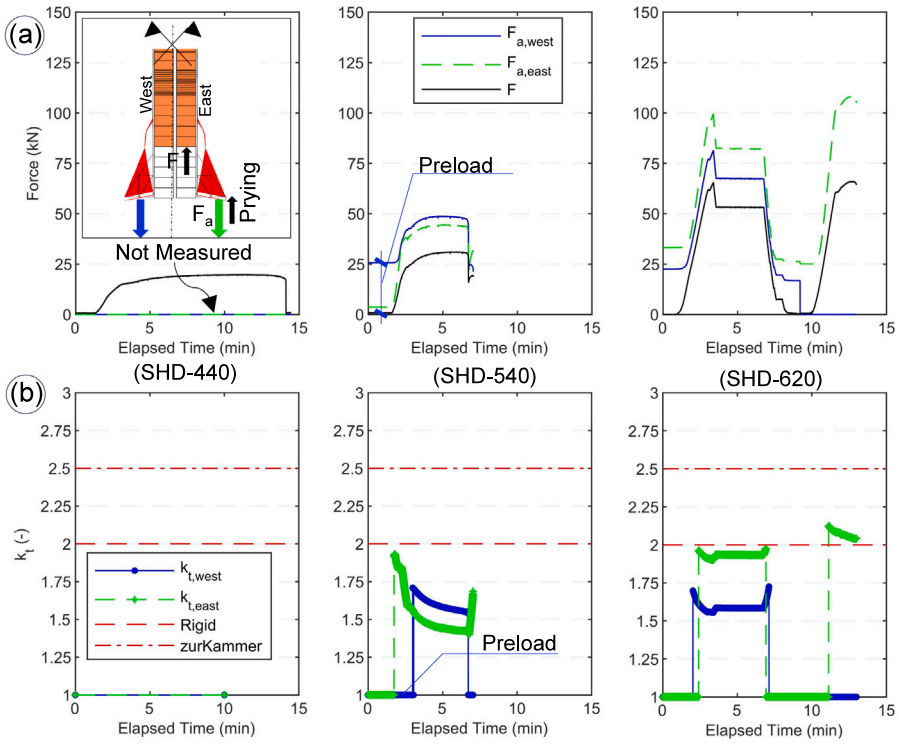

Fig. 10. Experimentally-derived eccentricity ratio (k_t) according to Eq. (2) for SHD tested statically: (a) forces at anchors; (b) k_t. (Notes. The Reader is referred to the color version of this figure.)

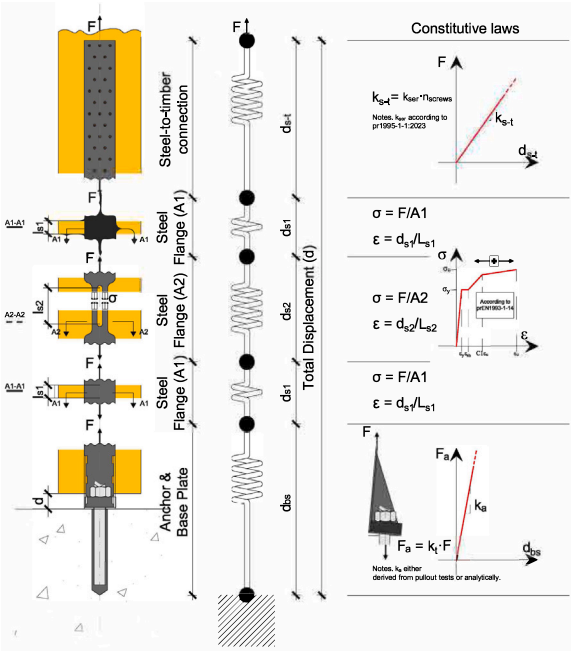

Fig. 11. Analytical model for hold-down connection using series of mechanical springs. (Notes. The Reader is referred to the color version of this figure.)

found when comparing analytically-derived stiffness and the experimental one.

For SHD, four are the major components which contributes to both the overall strength and stiffness in up-lift direction, i.e. anchorage-to-concrete and base plate, two segments of the vertical flange characterized by gross area (A1), the fuse (A2), the steel-to-timber connection.

To implement the simplified analytical model, the following general assumptions were made:

- Only up-lift monotonic load is considered as it was assumed for static experimental characterization.
- The total up-lift displacement of the hold-down connection (d) is analytically-derived as the summation of contributions given by the abovementioned four components according to Eq. (5):

$$d = d_a + d_{s1} + d_{s2} + d_{s-t} \tag{5}$$

where d_a is the anchor's displacement, i.e. slip between anchor and concrete foundation; d_{s1} and d_{s2} are displacements caused by the axial elongation of the SHD vertical flange in the A1 and A2 portions, respectively; d_{s-t} is the slip between SHD vertical flange and timber post. Such definition of d allows a consistent comparison with respect to experimentally-derived cross-head displacement (presented in Section 2.3).
- The stresses' state of the SHD vertical flange in the portions A1 and A2 is supposed to be uniform in tension, so is the state of deformations. Deformations between rows of screws as well as local plasticization possibly due to bearing are neglected.
- Due to vertical equilibrium, all components share the same up-lift force (F) with exception of the anchor's force (F_a) which is evaluated according to Eq. (1).
- The fuse component (A2 portion of the vertical flange) is characterized by elastic–plastic with hardening constitutive law according to [60]. The remaining three components are characterized by linear-elastic constitutive laws as further specified in the following.
- F and d are analytically-derived imposing subsequent steps of elastic–plastic evolution of the fuse, i.e. yielding, hardening, breaking.

Each component is now examined further.

- (Anchorage and Base Plate) The stiffness of the component is assimilated to the one of the anchor (k_a). Base plate and triangular stiffeners are

assumed infinitely rigid. k_a = 30 kN/mm was obtained from pullout tests for SL. For BO, due to absence of unconfined pullout tests, k_a was analytically-derived as $k_a = E \cdot A_b/h_{eff}$ where A_b and h_{eff} are the bolt's area and embedment depth, respectively. Displacement of the component (d_a) is equal to F_a/k_a, with F_a according to Eq. (1).

- (Steel-A1) The component is assimilated to uniformly stressed panel with $\sigma = F/A_1$ and $\epsilon = \sigma/E_s$ where A_1 is the gross area of the flange. The component is assumed linear-elastic before and after yielding of the fuse. Displacement of the component (d_{s1}) is equal to $\epsilon \cdot L_{s1}$.
- (Fuse [Steel-A2]) Similarly to the component A1, $\sigma = F/A_2$ where A_2 fuse's area. When yield stress is reached the stress-to-strain constitutive law follows the elastic–plastic with hardening model proposed in [60] thus ϵ takes values up to, say, 15 to 20%. Mean values of yielding (f_{ym}) and ultimate stresses (f_{um}) were simply assumed as 1.10 times characteristic ones. Although the Authors are aware about the roughness of such assumption, it revealed to be consistent with respect to larger statistical characterization given in [57]. Displacement of the component (d_{s2}) is equal to $\epsilon \cdot L_{s2}$.
- (Steel-to-timber connection) Both strength and stiffness of the component are characterized according to [47] by considering the connection as (i) a single shear plane; (ii) loaded parallel to the grain and (iii) with acting load level below the predicted load capacity according to European Yield Model [27]. Under these hypotheses, stiffness (k_{s-t}) is the summation, over the number of the connector, of the slip modulus ($K_{SLS,v}$). For screws, $K_{SLS,v} = 60(0.7d)^{1.7}$. Displacement of the component (d_{s-t}) is equal to F/k_{s-t}.

Fig. 12 shows the contributions (relatives) of each component to Eq. (5) for different stages of the fuse's elastic–plastic behavior; further numerical details are given in Appendix B. It is worth noting that, before the fuse yields, major contribution to displacement is given by both steel-to-timber connection and anchor. As expected, after yielding the displacement is dominated by plastic strains of the fuse.

Comparison between analytically-derived load-to-displacement curves and experimental ones is given in Fig. 8. Generally, results are comparable for all SHD (largest difference are found for SHD-620) by considering both static and cyclic tests. For the latter skeleton curves at cycle I have been considered. However, it is worth to mention that in all cases the experimental yielding was always over-strong with respect to analytical prediction whereas such difference was mitigated for ultimate strength. Besides, analytical model predicts ultimate displacements lower than experimental ones.

Finally, the presented analytical model should be considered in the largest context of non-linear multi-spring elements approach [61] as a tool for structural analysis of CLT seismic-resistant buildings. In such a case, the constitutive law of the non-linear spring should take into consideration both load inversion with buckling of the fuse and hysteretic cycles. For example, buckling can be treated with simplified lumped plasticity model [62]. Cyclic behavior of steel might be modeled assuming provisions in [63]. However, to the Authors' opinion, such enhancements are not easy-to-handle and generally they may not lead considerable reduction of computational costs if compared to explicit FEM which includes both geometrical and material non-linearities. In this light, cyclic response of hold-down with particular emphasis on the unloading path (where buckling was expected) was investigated using a three-dimensional FEM, as it is discussed subsequently in Section 3.2.

3.2. Finite-element model

A numerical investigation addressing SHD-540 was carried out to evaluate the influence of buckling of the fuse on the hysteretic behavior. For the sake of brevity, SHD-440 and SHD-620 were not considered in the numerical investigation but it is expected to apply similar discussion for the numerically-derived mechanical behavior. The sub-assemblage, as shown in Fig. 13, is modeled using three-dimensional finite elements as specified in the following. Commercial finite-element code [64] was used for the numerical analysis adopting standard Newton–Raphson [65] method for solution of non-linear equations. Both material (e.g. elastic–plastic steel) and geometrical (e.g. large displacement due to buckling) non-linearities were considered. Tolerances for convergence were set to $10^{(-2)}$ both for residual forces and displacement increments with maximum number of iterations equal to 100.

Steel plate was modeled using shells elements (quadrilateral and triangular) assuming non-linear material, i.e. elastic–plastic with hardening steel having stresses-to-strains diagram according to [60]. To promote the comparison with respect to experimental results, mean values were adopted for material parameters, i.e. for S355JR steel class f_{ym} = 391 MPa f_{um} = 561 MPa. Initial imperfection equal to $L_f/250$ was assumed according to [60]. Specifically, the initial deformed configuration was obtained magnifying the nodes' displacements of the buckling mode associated to bending of the fuse up to $L_f/250$ in the middle.

A reduced volume of the glulam timber post used in the experimental tests was adopted considering as relevant only the part in which screws were embedded, i.e. 50 mm. Such embedment length roughly coincided with thickness of the lamellas, i.e. 45 mm. Given the prevalent load direction parallel to the grains, the timber layer was modeled with brick elements using isotropic material. The elastic modulus, parallel to grains, of glulam Gl24 h was assumed according to [43], i.e. $E_{0\ g,mean}$ = 11.5 GPa. Poisson ratio was assumed according to Annex O of [47], i.e. $\nu = 0$. A fictitious friction pad was interposed between steel plate and timber having Mohr–Coulomb friction law characterized by cohesion (c) equal to 0.5 MPa and friction angle (Φ) equal to 30°. It is worth mentioning that c was tuned with respect to experimental results whereas $\Phi = 30°$ roughly corresponds to a friction coefficient (μ) equal to 0.58. Such value is consistent with experimental observations [66] of steel-to-timber interfaces, although it is larger than $\mu = 0.25$ commonly assumed for laterally-loaded connection [67].

Screws were modeled using linear-elastic beams elements with circular cross-section. To simulate the embedment condition, kinematic constraints (master–slave) were assigned to the beams taking inspiration from "no-explicit bolt-hole" modeling concept [68]. Specifically, on one beam's end the node has the same displacements of the nodes which discretized the hole in the steel plate, same approach for timber was used on the other beam's end. The Authors are aware that such modeling of connectors (screws) does not possess enough accuracy such as the one proposed, for example, in [69–71] which explicitly take into account distributed bearing and friction between connectors (nails in those cases) and surrounding timber. However, two were the encouraging experimental evidences upon which the simplification was based: on one hand, there was no evidence of bearing failure; on the other, screws did not show discernible plasticization.

At base plate, anchorage to concrete was modeled using a linear-elastic axial spring with stiffness equal to 30 kN/mm as obtained from pull-out test of single anchor. Spring was attached to the base plate with a single node neglecting the presence of the hole. No preload was applied to the anchor. Hard-contact between base-plate and concrete was modeled using compression only springs with stiffness evaluated according to [72]. Besides, to reduce the computational effort, the base plate and its attached triangular stiffeners had larger mesh size with respect to the other parts of the model. Such reduction of the level of approximation was allowed by experimentally-observed rigid behavior of the base plate. In fact, the base plate stiffness was increased by the presence of thick washer, as shown Fig. 6.c.

While in the general context of non-linear structural analysis, epistemic uncertainties possibly caused by different numerical modeling strategies [73] (e.g. sub-modeling, compatibility of displacements, material constitutive laws) may change failure modes, it is worth to remark that given the presence of steel fuse in the addressed structure as well as the uni-axial load condition such uncertainty is drastically reduced.

Comparison of numerical results and experimentally-derived ones, for static test, is shown in Fig. 14.a. Agreement is found for global

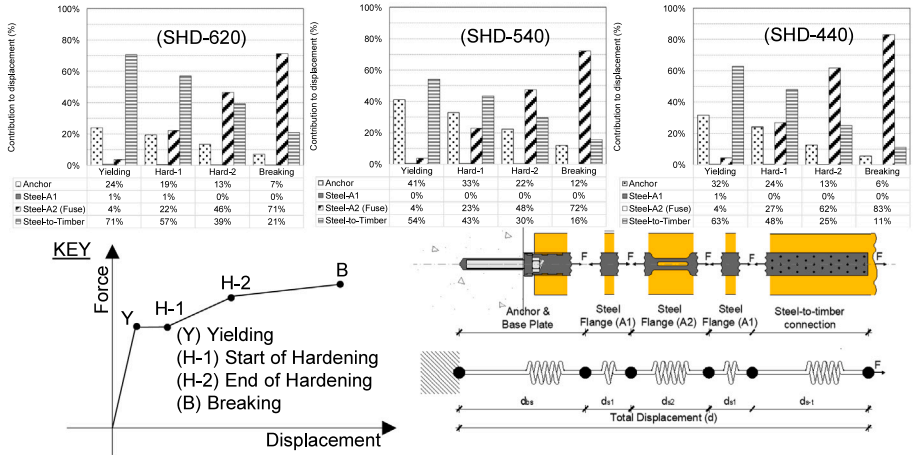

Fig. 12. Relative contributions to Eq. (5) given by components of simplified analytical model. (Notes. The Reader is referred to the color version of this figure.)

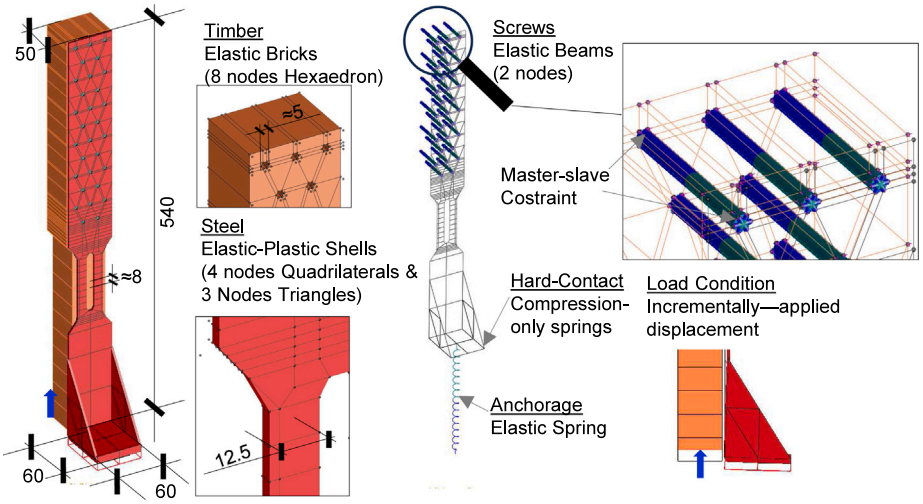

Fig. 13. Three-dimensional finite-element model of SHD-540. (Notes. Dimensions are given in millimeters. The Reader is referred to the color version of this figure.)

response, although the numerically derived maximum load is slightly lower with respect to experimental one. Such difference might be attributed to a conservative estimate for both f_{ym} and f_{um}. Numerically-derived F_a is shown in Fig. 14.b. A similar k_t with respect to analytical model is found, i.e. $k_t = 2.0$ according to Eq. (2). Steel-to-timber connection is characterized by larger numerically-derived slip with respect to experimental results as shown in Fig. 14.c. Finally, as shown in Fig. 14.d, it is worth to mention that strains at fuse reached values up to 25% which was set as ultimate strain for steel's constitutive law. Larger values were considered as a consequence of numerical inaccuracy in stresses and strains recovering [74].

Fig. 15.a shows the numerical results obtained for cyclic test. For up-lift direction, numerically-derived load-to-displacement curve agrees with respect to experimental results. Besides, as can be inferred from Fig. 15.b, differences for local displacements have the same magnitude as the ones previously discussed for static test. Numerical failure was obtained having exceeded the assumed tolerance limit for residual forces, i.e. 10^{-2}.

As expected, numerical hysteretic behavior deviates from experimental for unloading paths, i.e. when the cross-head displacement varies from a target up-lift to zero. Indeed, it is proven that the fuse buckles in the first unloading cycle at a load level comparable to the critical load (shown in Fig. 16.b.) if analytically evaluated using Second Order Theory, e.g. by adapting to an elastic–plastic beam the buckling load given for an elastic one [75]. It is worth to mention that buckling displacements shown in Fig. 16.a reach values which are almost equal to one-half of the buckling length. Cycles subsequent to first buckling are characterized by development of plastic hinge associated to large strains as shown in evolutionary plots of Fig. 16.c/d.

Buckling during unloading is responsible for loss of strength for two subsequent cycles at the same target of up-lift displacement. In fact, during reloading part of the energy is spent to straighten the fuse which underwent inelastic buckling shape. Comparison of the impairment of strength (φ_{imp}) is given in Table 4. For the sake of completeness, the Table includes analytically-derived nominal ductility (μ) considering an equivalent-energy elastic–plastic model (EEEP) [58]. According to [5], φ_{imp} should be limited to 30% for dissipative connections of timber structures. Besides, a strength reduction (k_{deg}) not smaller than 0.8 is prescribed. The same post-processing was applied to a traditional hold-down tested cyclically by [22], but results are discussed in Section 3.3.

For SHD-540, both numerically-derived and experimental load-to-displacement skeleton curves at cycle I can be converted to an EEEP characterized by μ equal to 4.0 ($\mu > 1.5$ is prescribed in [5]) and almost equal yield loads and displacements. For ductility demand $\mu > 2.5$, both strength reduction and impairment of SHD are within the conventional thresholds. The limit for φ_{imp} is slightly exceeded for numerically-derived strength when $\mu > 3$. As mentioned before, flexural plastic hinge consequent to buckling is mainly responsible for such impairment.

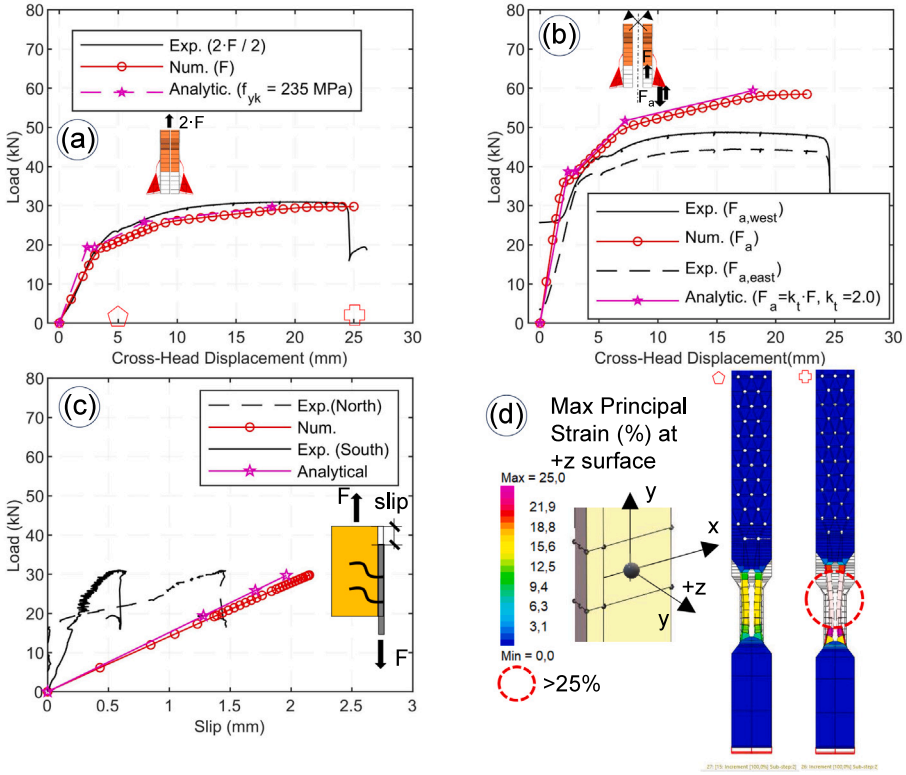

Fig. 14. Numerically-derived results for SHD-540 tested statically: (a) load-to-displacements; (b) anchors' forces; (c) slip between steel plate and timber post; (d) strains at fuse. (Notes. In (d) strains are referring to values at centroid of the elements. The Reader is referred to the color version of this figure.)

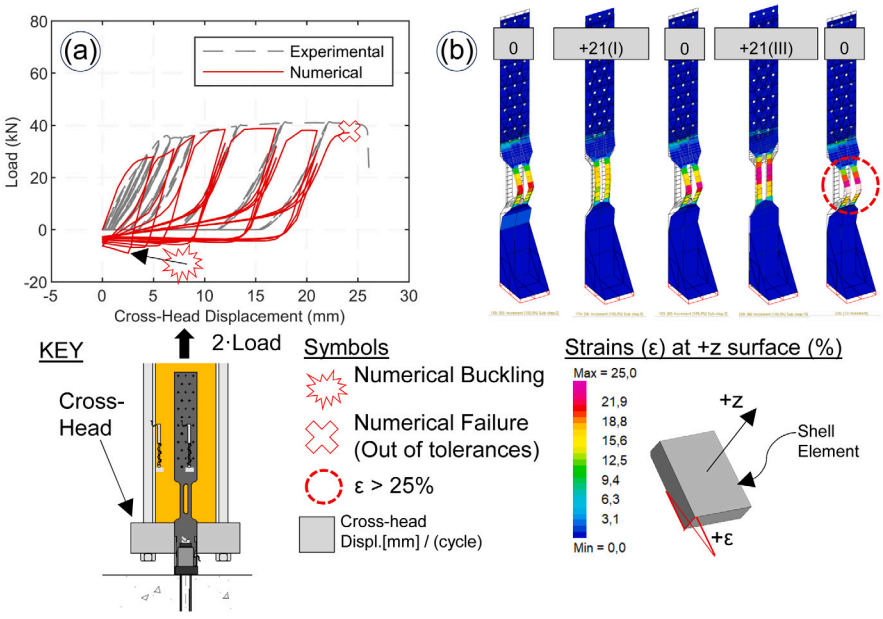

Fig. 15. Numerically-derived results for SHD-540 tested cyclically: (a) load-to-displacements curves; (b) contour plots of strains. (Notes. In (b) displacements have been magnified for representation purpose. The Reader is referred to the color version of this figure.)

Whether buckling should be allowed for dissipation zones in CLT buildings, such as hold-down, is controversial. On one hand, since buckling of the vertical flange is not considered in typical capacity-design provisions [5], assuming it in design is somehow not recommended at the date.

On the other, the Authors were encouraged by the similarity of mechanical behavior of SHD with respect to diagonals elements adopted for steel bracings [77]. In this case, buckling of compressed diagonals is allowed providing that the diagonal in tension has sufficient dissipation capacity. In the same way, a pair of SHD devices (one in tension and one buckled) may be designed to withstand the overturning moment at the corners of a CLT wall.

Generally, when buckling occurs in alternate cycles, the resulting hysteretic behavior is characterized by pinching. For SHD there is one favorable condition, i.e. cycles are not completely alternate because when hard-contact is reached between panel and concrete foundation,

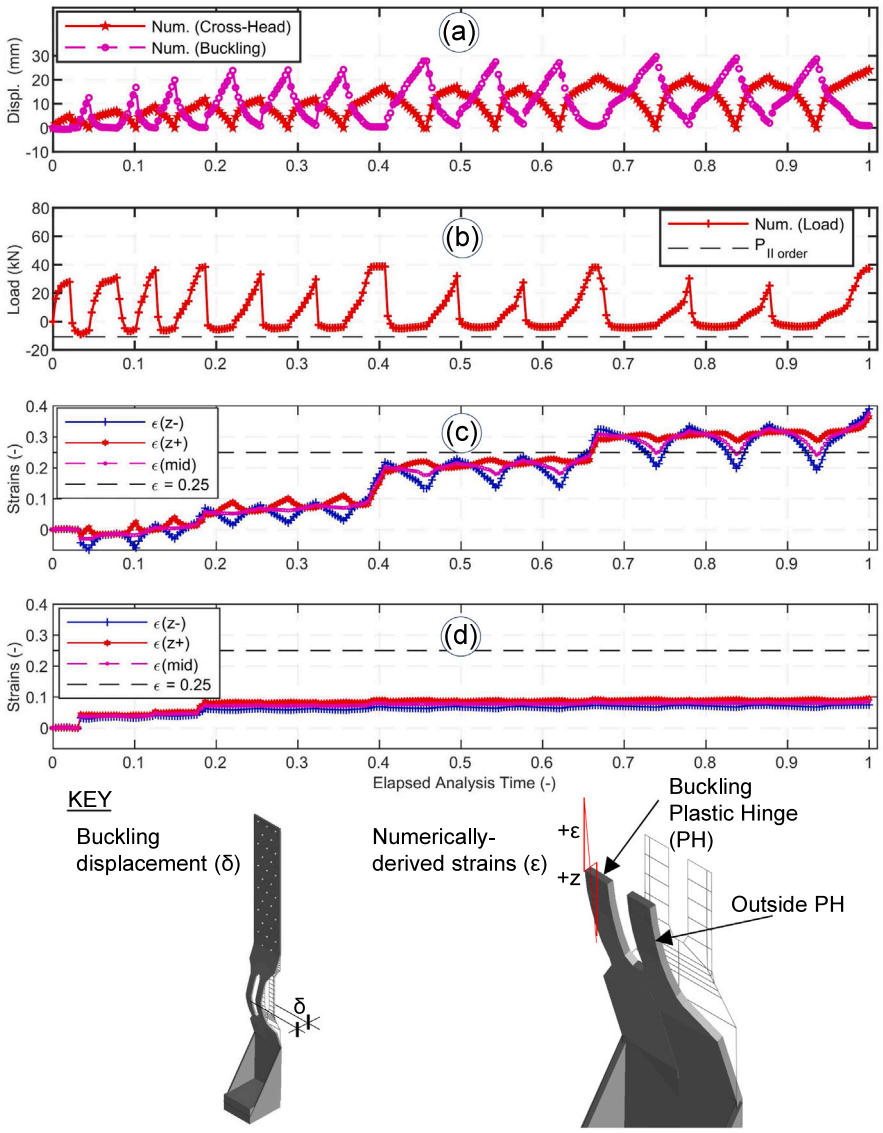

Fig. 16. Numerically-derived time histories for SHD-540 tested cyclically: (a) buckling displacements; (b) vertical force; (c) strains at plastic hinge; (d) strain outside plastic hinge. (Notes. The Reader is referred to color version of this figure.)

compression is no longer transferred by the vertical flange. However, for SHD two questions remains: (i) how much buckling influences the tension capacity? (ii) might low-cyclic fatigue be an issue? The answers are given in the following mainly based on what the Authors found in [78].

First, the performance depends on the deformation history. For what has been numerically-observed, in case of an ascending displacement protocol (which commonly characterizes structures far from earthquake sources) reduction of both strength and ductility was not significant. Second, the number of cycles withstood by a structure during earthquake ranges from 5 to 20 thus the notion of fatigue is questionable as much as such steel's crack generated under earthquake should be considered as ductile crack, not as fatigue crack. Such intuition was generally confirmed [79] by cyclic tests of notched dog-bone specimens, at constant amplitude. Cracks characterizing cyclic tests with combined large plastic strains and low number of cycles (e.g. 100 cycles and $6\epsilon_y$, where ϵ_y was the strain at yielding) had similar fractographs (ductile crack) to the ones associated to monotonic reference tests. Different fractographs (fatigue crack) were observed for high number of cycles and reduced plastic strains. For SHD, ductile crack is expected thus nominal ultimate strain of steel can be assumed albeit the effect of strains' gradient at buckling plastic hinge should be investigated further.

3.3. Comparing SHD to a traditionally-designed hold-down

A final comparison is given between SHD and a traditional hold-down, i.e. designed such that ductile failure is promoted at steel-to-timber connection. To the scope, SHD-540 is compared to WHT-540 tested in [22] which geometry is specified in [80]. Load-to-displacement curve for WHT-540 is available as an example file of freeware software So.ph.i [61], accessed at http://giovanni.rinaldin.org in January 2024. Failure was attributed to combined embedment in timber and formation of plastic hinge in nails along with partial withdrawal.

Fig. 17 shows the comparison between SHD-540 and WHT-540, both tested cyclically. Major inelastic mechanisms, characterizing the two hold-downs, are illustrated as well. The loads are scaled by F_y analytically-derived using EEEP envelopes [58]. Among possible EEEP which satisfy energy equivalence with respect to skeleton curve at first cycle (with tolerance set to 10^{-2}), selection was made to the ones which are characterized by almost the same parameters for both SHD-540 and

Table 4
Strength's reduction, strength's impairment and equivalent viscous damping for SHD-540 and WHT-540, tested cyclically.

		SHD-540 (This paper)					WHT-540 [22]			
		Experimental		Numerical			Experimental			
EEEP										
d_y	(mm)	6.0		6.0			5.0			
F_y	(kN)	35.0		37.0			40.0			
μ	(–)	4.0		4.0			4.0			
Strength reduction ($k_{deg} = F_u/F_{max}$) [5]										
F_{max}	(kN)	41.3		38.7			50.2			
F_u	(kN)	41.3		37.0			47.0			
k_{deg}	(–)	1.00		0.96			0.94			
Strength impairment ($\varphi_{imp} = F_i/F_1$) [5] *and Equivalent viscous damping* (ζ_{eq}) [76]										
d (mm)	Cycle (–)	F_i (kN)	φ_{imp} (–)	F_i (kN)	φ_{imp} (–)	ζ_{eq} (%)	d (mm)	F_i (kN)	φ_{imp} (–)	ζ_{eq} (%)
12.0	d/d_y		2.0		2.0		6.0		1.2	
	I	39.6	0.00	38.0	0.00	11%		25.8	0.00	9%
	II	38.6	0.03	33.2	0.13	5%		24.3	0.06	5%
	III	37.7	0.05	29.8	0.22	5%		23.1	0.10	5%
17.0	d/d_y		2.8		2.8		11.9		2.4	
	I	40.6	0.00	38.7	0.00	12%		40.1	0.00	14%
	II	39.8	0.02	32.0	0.17	5%		37.9	0.05	4%
	III	39.4	0.03	27.5	0.29	5%		36.2	0.10	4%
21.0	d/d_y		3.5		3.5		Failure at subsequent cycles.			
	I	40.9	0.00	38.2	0.00	8%				
	II	40.1	0.02	30.3	0.21	5%				
	III	39.1	0.04	25.3	0.34	6%				

WHT-540, i.e. $\mu = 4.0$, $F_y \approx 40$ kN, $d_y \approx 5$ mm. For cycles characterized by $\mu > 1$, equivalent viscous damping (ζ_{eq}) was analytically-derived according to [76] adapting the general definition to semi-cyclic response [81]. Numerical values obtained post-processing the experimentally-derived results are given in Table 4.

If the up-lift phase is considered, e.g. 10 mm target displacement is conveniently assumed in Fig. 17, SHD-540 mainly develops plastic strains in the fuse whereas WHT-540 behavior is characterized by plastic bending of nails which simultaneously embed in the surrounding timber. When displacement is recovered (e.g. 5 mm) both the devices show pinching of the hysteretic behavior, i.e. non-zero displacements associated to almost zero load. However, for the two considered cases pinching has different inelastic sources. Indeed, buckling of the fuse characterizes SHD-540 with residual compressive reaction ($F^{(-)}$) caused by second order effects. For WHT-540 recover of inelastic slip caused by timber's embedment occur and $F^{(-)}$ is mainly caused by inverse flexural yielding of the nails.

A further confirmation of the limited hysteretic resources for both SHD and WHT can be obtained from ζ_{eq} which roughly varies from 0.10 at first cycle to 0.05 at subsequent cycles of same ductility demand. In fact, only the first cycle is characterized by yielding therefore definition of hysteretic damping according to [76] may apply. Conversely, subsequent cycles can be crudely interpreted as elastic (non-linear) unloading and reloading which are typically characterized by the so called "elastic damping", i.e. $\zeta_{eq} = 0.05$. To summarize, pinching of hysteretic behavior characterizes both SHD and traditional hold-down although the inelastic mechanisms are different. Two more considerations are worth to mention although they are hypothetical. First, if for SHD less overstrength is assumed for steel-to-timber failure mechanism, e.g. by reducing the number of screws, slip between steel and timber might increases, during up-lift, as a consequence of connectors' embedment. In such a case, during recovering of both slip and fuse's plastic deformations, buckling of SHD is either postponed to cycles at high ductility demand (e.g. $mu = 2$) or, depending on the amount of slip, even prevented.

Second, for a traditional hold-down when withdrawal of connectors is simultaneous to their lateral failure as often observed in experimental tests [22], the vertical flange becomes unrestrained to buckling in compression. Such issue, mainly inspired by experimental evidence shown in Fig. 2.e, should receive more attention in traditionally-designed hold-down devices.

4. Conclusions

An new hold-down device (SHD) was designed for applications to seismic-resistant CLT buildings. Essentially, ductile failure of a reduced segment (fuse) of the vertical flange is assumed as design concept. Experimental results as well as the discussion presented in this paper allow to make some general conclusions as it follows.

1. SHD shows ductile (μ larger than 3) axial behavior mainly dependent on plastic elongation of the fuse. Such behavior is consistent to the expected performance of hold-down devices used to restrain seismic overturning of CLT walls. Stiffness of the connection as well as load-carrying capacity were analytically-derived using an application of the component method. Although validation was given only for monotonic up-lift load case, extension to cyclic load is possible. Each component was characterized, with a certain amount of engineering judgment, following provisions of the Second Generation Eurocodes. The proposed analytical definition of SHD can be used within the framework of multi-spring approach usually adopted for structural analysis of CLT buildings.
3. Buckling of the fuse occurs while recovering up-lift displacement during cycles. The issue was observed numerically and further experimental–numerical investigations are needed to evaluate the impact of buckling at the scale of a CLT wall. In practical circumstances, it is recommend to design SHD devices similarly to diagonal elements of steel bracings, i.e. neglecting the contribution of the compressed element.
3. Although inelastic mechanisms are different, comparable hysteretic behaviors are recognized for SHD with respect to traditionally-designed hold-down surveyed from literature, i.e. designed such that yielding of connectors (e.g. nails or screws) combined to timber's embedment is promoted. Both devices are affected by pinching of hysteretic cycles that is mainly caused by buckling of the fuse for SHD and by timber's embedment for traditional hold-down. Further, non significant differences of ductility, impairment of strength as well as equivalent viscous damping are recognized.

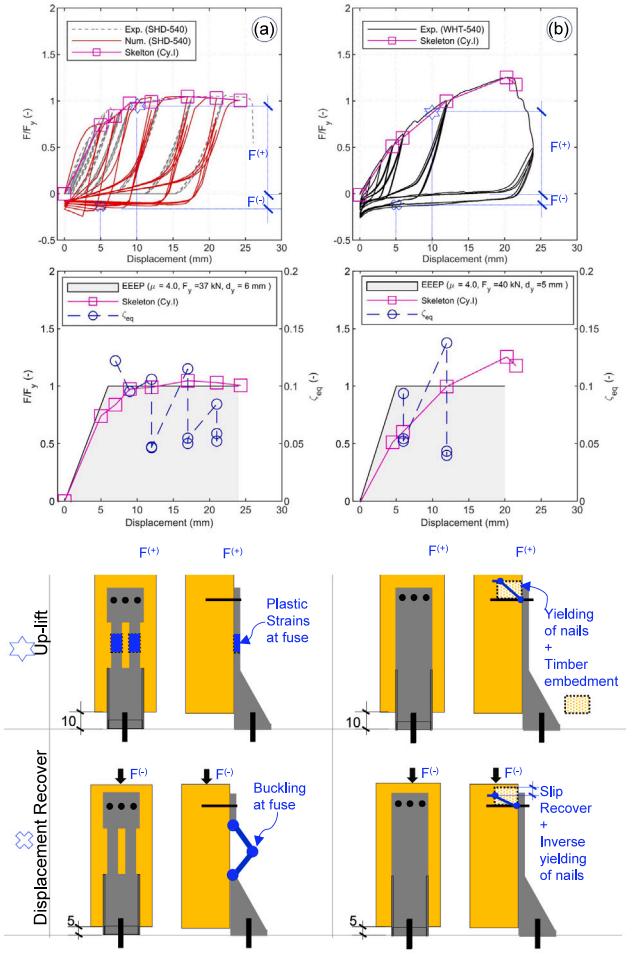

Fig. 17. Comparison between SHD and traditionally-designed hold-down tested cyclically: (a) SHD-540; (b) WHT-540 [22]. (Notes. In sketches, only one row of connectors is shown and displacements were exaggerated for representation purposes. (ζ_{eq}) is the equivalent viscous damping. The Reader is referred to the color version of this figure.)

CRediT authorship contribution statement

A. Marchisella: Writing – review & editing, Writing – original draft, Visualization, Validation, Software, Resources, Methodology, Investigation, Formal analysis, Data curation, Conceptualization. **G. Muciaccia:** Writing – review & editing, Methodology, Conceptualization.

Declaration of competing interest

The authors of the manuscript declare no conflict of interest.

Data availability

Data will be made available on request.

Acknowledgments

The experimental part of the presented study was financially supported by Friuslsider S.P.A. Tests were carried out at Testing Lab. for Materials, Buildings and Civil Structures of the Politecnico di Milano.

Appendix A. Analytically-derived axial strengths

See Table A.5.

Appendix B. Analytically-derived forces and displacements using simplified analytical model

See Table B.6.

Appendix C. Extended analytical derivation of anchor's force

C.1. Analytical developments

Equilibrium and compatibility of displacements of hold-down baseplate subjected to up-lift are analytically-derived, in the following, considering the notation used Fig. C.18. Such analytical developments expand the approximate definition of the anchor force (F_a) given by Eq. (1).

- Equilibrium to vertical translation:

$$F + F_P = F_a \tag{C.1}$$

- Equilibrium to horizontal translation:

$$V_{fl} = V_{fr} + V_a \tag{C.2}$$

- Equilibrium to rotation around point P:

$$F_a \cdot b/2 + (M_{fl} - V_{fl} \cdot h_{st}) = F(b-u) \tag{C.3}$$

Equilibrium of the fuse segment (h_{fu}) implies:

$$2 \cdot M_f = V_f \cdot h_{fu} \tag{C.4}$$

According to compatibility of displacements, horizontal displacement (u) and vertical displacement (δ_f) are related as it follows:

$$u = atan\left(\frac{\delta_f l}{b}\right) \cdot h_{st} \approx \frac{\delta_f}{b} \cdot h_{st} \tag{C.5}$$

Yet, the anchor's displacement can be written as it follows:

$$\delta_a = 1/2 \cdot \delta_f \tag{C.6}$$

The constitutive law of anchor is written as it follows:

$$F_a = k_a \cdot \delta_a \tag{C.7}$$

By combining previous equations, F_a can be re-written as it follows:

$$F_a = \frac{2 \cdot F - 2 \cdot (M_f/b - V_f \cdot h_s t/b)}{1 + \frac{4 \cdot N}{k_a \cdot b}} \tag{C.8}$$

C.2. Numerical example: SHD-540

Data

- $h_{fu} = 70$ (mm);
- $b = 70$ (mm);
- $h_{st} = 105$ (mm);
- $M_f = 1/4 \cdot 3^2 \cdot 25 \cdot 235 = 13\,219$ (N mm), (at flexural yielding);
- N = from 5000 to 20 000 N;
- k_a = from 10 000 to 50 000 N/mm;

Results

Tables C.7 and C.8 report the ratio $F_a/F = k_t$ using Eq. (C.8) either neglecting or not the contribution of M_f and V_f. Values associated to SHD-540 are given in bold phase. Results are comparable with $k_t = 2.00$ which was approximately assumed in Eq. (2) both by (i) neglecting M_f in equilibrium and (ii) $k_a \approx \infty$.

Table A.5
Analytically-derived up-lift strengths for SHD considering different type of failure mechanisms.

SHD	620	540	440		Description/Formulas
Steel tensile break-out					
A_f	136	75	50	(mm^2)	
$N_{yk,steel}$	32	18	12	(kN)	$N_{yk,steel} = A_f \cdot f_{yk}$
$N_{uk,steel}$	49	27	18	(kN)	$N_{uk,steel} = A_f \cdot f_{uk}$
γ_{M2}		1.25		(–)	Partial factor for material for the case of resistance of cross-sections in tension according to [47]
$N_{Rd,steel}$	39	22	14	(kN)	$N_{ud,steel} = \frac{N_{uk,steel}}{\gamma_M}$
Buckling during un-loading path					
l_0	72	80	80	(mm)	Buckling length
J	102	56	26	(mm^4)	Inertia in weak axis
λ	83	92	111	(–)	$\lambda = l_0/\sqrt{\frac{J}{A}}$
γ_{M1}	1.00			(–)	Partial factor for material for instability according to [48]
$N_{b,Rd}$	39	17	8	(kN)	$N_{b,Rd} = \pi^2 \frac{E \cdot J}{l_0^2 \cdot \gamma_{M1}}$
γ_{M0}		1.00		(–)	Partial factor for material for pure compression according to [48]
$N_{c,Rd}$	49	27	18	(kN)	$N_{c,Rd} = \frac{A_f \cdot f_{uk}}{\gamma_{M0}}$
$\frac{N_{b,Rd}}{N_{Rd,c}}$	0.79	0.64	0.45	(–)	–
Failure of laterally loaded screws (without effective numbers)					
F_{vrk}	1.9	1.9	1.9	(kN)	According to ETA
n_{tot}	45	30	20	(–)	Total number of screws
$F_{vrk,tot}$	86.4	57.6	38.4	(kN)	$F_{vrk,tot} = F_{vrk} \cdot n_{tot}$
γ_R	1.30			(–)	Partial factor for connections according to [47].
$F_{vRd,tot}$	66.5	44.3	29.5	(kN)	$F_{vRd,tot} = \frac{F_{vrk,tot}}{\gamma_R}$
$\frac{F_{vrd,tot}}{N_{Rd,steel}}$	1.69	2.05	2.05	(–)	–
Failure of laterally loaded screws (with effective numbers)					
Ψ_{eff}	0.6	0.7	0.7	(–)	Effective screws factor according to [47]
$\frac{F_{vrd,tot} \cdot \Psi_{eff}}{N_{Rd,steel}}$	0.98	1.41	1.53	(–)	–
Plug shear failure					
l_{con}	445	302	202	(mm)	–
f_{vk}		3.50		(MPa)	Characteristic shear strength according to [43]
γ_M		1.25		(–)	Partial factor for timber material according to [47]
k_{mod}		1.00		(–)	Modification factor (instantaneous loads) according to [47]
f_{vd}		2.80		(MPa)	$f_{vd} = k_{mod} \frac{f_{vk}}{\gamma_M}$
t_{ef}	40	40	40	(mm)	$F_{vrk,tot} = F_{vrk} \cdot n_{tot}$
k_v		0.72		(–)	Reduction factor for shear according to [47]
$F_{v,la,d}$	90.3	61.3	41.0	(kN)	$F_{v,la,d} = 2 \cdot k_v t_{ef} f_{vd} l_{con}$ according to [47]
$\frac{F_{v,la,d}}{N_{Rd,steel}}$	2.30	2.84	2.85	(–)	–
Anchorage-to-concrete failure (single anchor un-disturbed)					
k_t		2.0		(–)	Eccentricity factor according to Fig. 3
Type	BO	SL	SL	(–)	BO—Bonded anchor; SL—Sleeve anchor
d	20	24	20	(mm)	Anchors' diameter
h_{eff}	350	150	100	(mm)	Embedment depth
$\tau_{Rk,c}$	5.7	–	–	(MPa)	Characteristic shear strength for C1 seismic condition according to [52]
k_1	7.7	7.7	7.7	(–)	Concrete cone factor (cracked concrete)
$N_{rk,c0}$	225.5	63.3	34.4	(kN)	Concrete-cone capacity for single anchor according to [51], i.e. $N_{rk,c0} = k_1 h_{eff}^{1.5} f_c^{0.5}$
$N_{rk,p0}$	125.3	–	–		Pullout capacity for single anchor according to [51], i.e. $N_{rk,p0} = \pi d h_{eff} \tau_{rk}$
f_c	20	20	20	(MPa)	Concrete compressive strength
$N_{rk,1}$	125.3	63.3	34.4	(kN)	Tensile capacity for single anchor according to [51]
γ_{Mc}		1.50		(–)	Partial factor for concrete-related failure for anchorages according to [51]
γ_{eq}		1.10		(–)	Partial factor for seismic situation according to Annex G of [54]
$N_{Rd,1}$	76.0	38.3	20.9	(kN)	$N_{rd,1} = \frac{N_{rk,0}}{\gamma_{Mc} \gamma_{eq}}$
$\frac{N_{Rd,1}}{k_t \cdot N_{uRd,steel}}$	0.97	0.89	0.72	(–)	–

Table B.6
Analytically-derived forces and displacements, for SHD devices, according to springs model presented in Fig. 11.

SHD		620					540					440				
Global behavior																
F	(kN)	0.0	51.1	51.1	65.1	73.5	0.0	29.3	29.3	37.3	42.075	0.0	12.9	12.9	17.2	19.8
d	(mm)	0.00	3.19	3.95	7.30	15.35	0.00	3.57	4.46	8.33	17.70	0.00	2.04	2.67	6.78	17.57
Components' stiffness																
k_a	(kN/mm)	–	100	100	100	100	–	30	30	30	30	–	30	30	30	30
k_{s1}	(kN/mm)	–	1920	1920	1920	1920	–	1680	1680	1680	1680	–	1200	1200	1200	1200
k_{s2}	(kN/mm)	–	437	58	19	7	–	214	29	9	3	–	143	18	4	1
k_{s-t}	(kN/mm)	–	23	23	23	23	–	15	15	15	15	–	10	10	10	10
Components' displacements																
d_{sa}	(mm)	0.00	0.77	0.77	0.98	1.10	0.00	1.46	1.46	1.86	2.10	0.00	0.65	0.65	0.86	0.99
d_{s1}	(mm)	0.00	0.03	0.03	0.03	0.04	0.00	0.02	0.02	0.02	0.03	0.00	0.01	0.01	0.01	0.02
d_{s2}	(mm)	0.00	0.12	0.88	3.39	10.94	0.00	0.14	1.02	3.96	12.76	0.00	0.09	0.72	4.19	14.58
d_{s-t}	(mm)	0.00	2.25	2.25	2.87	3.23	0.00	1.93	1.93	2.46	2.78	0.00	1.28	1.28	1.71	1.96

Notes. Forces and displacements are given for different stages, i.e. undeformed, at yielding of the fuse, at the start and end of hardening phase for the fuse, at breaking of the fuse.

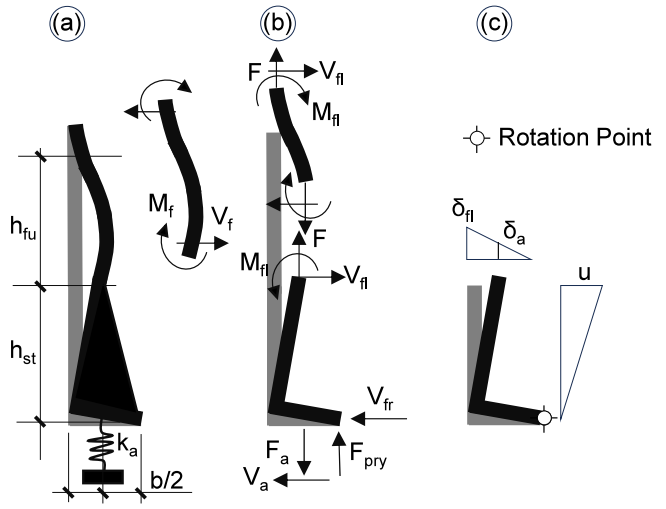

Fig. C.18. Detailed mechanical model to analytically-derive anchor's force (F_a): (a) geometry; free-body diagrams; (c) displacements' field. (Notes. Displacements were exaggerated for representation purposes.)

Table C.7
F_a/F neglecting M_f and V_f in Eq. (C.8).

F (N)	k_a (N/mm)				
	10 000	20 000	**30 000**	40 000	50 000
5000	1.94	1.97	1.98	1.99	1.99
10000	1.89	1.94	1.96	1.97	1.98
20000	1.79	1.89	1.93	1.94	1.96
30 000	1.71	1.84	**1.89**	1.92	1.93

Table C.8
F_a/F using Eq. (C.8).

F (N)	k_a (N/mm)				
	10 000	20 000	**30 000**	40 000	50 000
5000	2.06	2.09	2.10	2.11	2.11
10000	1.95	2.00	2.02	2.03	2.04
20000	1.82	1.92	1.96	1.97	1.99
30 000	1.72	1.86	**1.91**	1.94	1.95

References

[1] Oliver CD, Nassar NT, Lippke BR, McCarter JB. Carbon, fossil fuel, and biodiversity mitigation with wood and forests. J Sustain For 2014;33(3):248–75. http://dx.doi.org/10.1080/10549811.2013.839386.

[2] Tollefson J. Wood grows up. Nature 2017;545(7654):280–2. http://dx.doi.org/10.1038/545280a.

[3] van de Lindt JW. Evolution of wood shear wall testing, modeling, and reliability analysis: Bibliography. Pract Period Struct Des Constr 2004;9(1):44–53. http://dx.doi.org/10.1061/(asce)1084-0680(2004)9:1(44).

[4] Izzi M, Casagrande D, Bezzi S, Pasca D, Follesa M, Tomasi R. Seismic behaviour of cross-laminated timber structures: A state-of-the-art review. Eng Struct 2018;170:42–52. http://dx.doi.org/10.1016/j.engstruct.2018.05.060.

[5] prEN 1998-1-2. Eurocode 8 - Design of structures for earthquake resistance part 1-2: Buildings. 2023.

[6] Gazetas G. 4Th ishihara lecture: Soil-foundation-structure systems beyond conventional seismic failure thresholds. Soil Dyn Earthq Eng 2015;68:23–39. http://dx.doi.org/10.1016/j.soildyn.2014.09.012.

[7] Forcellini D. Seismic fragility of tall buildings considering soil structure interaction (SSI) effects. Structures 2022;45(September):999–1011. http://dx.doi.org/10.1016/j.istruc.2022.09.070.

[8] Stewart JP, Seed R, Fenves G. Seismic soil-structure interaction in buildings, II: Empirical findings. J Struct Eng (U S) 1999. http://dx.doi.org/10.1061/(ASCE)1090-0241(1999)125:1(3).

[9] Vicencio F, Torres-Olivares S, Flores EIS. An high order seismic study to evaluate the structure-soil-structure-interaction between adjacent CLT structures. 2024, http://dx.doi.org/10.2139/ssrn.4750620, SSRN.

[10] Vicencio F, Torres-Olivares S, Saavedra Flores EI. Structure-soil-structure interaction between a pair of cross-laminated timber buildings under seismic loads. In: Recent advances on the mechanical behaviour of materials. ICM 2023, Springer; 2024, http://dx.doi.org/10.1007/978-3-031-53375-4_1.

[11] Ceccotti A, Follesa M. Seismic behaviour of multi-storey xlam buildings. In: International workshop on earthquake engineering on timber structures. 2006, p. 81–95.

[12] Vassallo D, Follesa M, Fragiacomo M. Seismic design of a six-storey CLT building in Italy. Eng Struct 2018;175(2017):322–38. http://dx.doi.org/10.1016/j.engstruct.2018.08.025.

[13] Rinaldi V, Casagrande D, Cimini C, Follesa M, Fragiacomo M. An upgrade of existing practice-oriented FE design models for the seismic analysis of CLT buildings. Soil Dyn Earthq Eng 2021;149(2020):106802. http://dx.doi.org/10.1016/j.soildyn.2021.106802.

[14] Fragiacomo M, Dujic B. Elastic and ductile design of multi-storey crosslam massive wooden buildings under seismic actions. Eng Struct 2011;33(11):3043–53. http://dx.doi.org/10.1016/j.engstruct.2011.05.020.

[15] Lukacs I, Björnfot A, Tomasi R. Strength and stiffness of cross-laminated timber (CLT) shear walls: State-of-the-art of analytical approaches. Eng Struct 2019;178(2018):136–47. http://dx.doi.org/10.1016/j.engstruct.2018.05.126.

[16] Casagrande D, Rossi S, Sartori T, Tomasi R. Proposal of an analytical procedure and a simplified numerical model for elastic response of single-storey timber shear-walls. Constr Build Mater 2016;102:1101–12. http://dx.doi.org/10.1016/j.conbuildmat.2014.12.114.

[17] Aloisio A, Boggian F, Tomasi R, Fragiacomo M. The role of the hold-down in the capacity model of LTF and CLT shear walls based on the experimental lateral response. Constr Build Mater 2021;289:123046. http://dx.doi.org/10.1016/j.conbuildmat.2021.123046.

[18] Jorissen A, Fragiacomo M. General notes on ductility in timber structures. Eng Struct 2011;33(11):2987–97. http://dx.doi.org/10.1016/j.engstruct.2011.07.024.

[19] Gavric I, Fragiacomo M, Ceccotti A. A strength and deformation characteristics of typical X-lam connections. In: World conference on timber engineering 2012. WCTE 2012, Vol. 2, 2012, p. 146–55, (April 2019).

[20] EN 1998-1-1. Eurocode 8: Design of structures for earthquake resistance. Part1: General rules, seismic actions and rules for buildings. 2004.

[21] Follesa M, Fragiacomo M, Casagrande D, Tomasi R, Piazza M. The new provisions for the seismic design of timber buildings in Europe. Eng Struct 2018;168(May):736–47. http://dx.doi.org/10.1016/j.engstruct.2018.04.090.

[22] Gavric I, Fragiacomo M, Ceccotti A. Cyclic behaviour of typical metal connectors for cross-laminated (CLT) structures. Mater Struct/Mater Constr 2015;48(6):1841–57. http://dx.doi.org/10.1617/s11527-014-0278-7.

[23] Tomasi R, Sartori T. Mechanical behaviour of connections between wood framed shear walls and foundations under monotonic and cyclic load. Constr Build Mater 2013;44:682–90. http://dx.doi.org/10.1016/j.conbuildmat.2013.02.055.

[24] Dong W, Li M, Ottenhaus LM, Lim H. Ductility and overstrength of nailed CLT hold-down connections. Eng Struct 2020;215(February):110667. http://dx.doi.org/10.1016/j.engstruct.2020.110667.

[25] Liu J, Lam F. Experimental test of coupling effect on CLT hold-down connections. Eng Struct 2019;178(2018):586–602. http://dx.doi.org/10.1016/j.engstruct.2018.10.063.

[26] Pozza L, Ferracuti B, Massari M, Savoia M. Axial – shear interaction on CLT hold-down connections – Experimental investigation. Eng Struct 2018;160(2017):95–110. http://dx.doi.org/10.1016/j.engstruct.2018.01.021.

[27] Johansen KW. Theory of timber connections. Int Assoc Bridge Struct Eng 1949;9:249–62. http://dx.doi.org/10.5169/seals-9703.

[28] EN 1995-1-1. Eurocode 5: Design of timber structures — Part 1-1: General — Common rules and rules for buildings. 2004.

[29] Canetti D, Sartori T, Polastri A. Timber Buildings: a prefabricated solution for connection of the foudation (Italian). Struct Web 2020;230(19). http://dx.doi.org/10.12917/STRU230.19.

[30] Scotta R, Marchi L, Trutalli D, Pozza L. Engineered aluminium beams for anchoring timber buildings to foundation. Struct Eng Int 2017;27(2):158–64. http://dx.doi.org/10.2749/101686617X14881932435736.

[31] Scotta R, Trutalli D, Marchi L, Pozza L. On the anchoring of timber walls to foundations: Available strategies to prevent wood deterioration and on-site installation problems. Procedia Struct Integr 2018;11:282–9. http://dx.doi.org/10.1016/j.prostr.2018.11.037.

[32] Latour M, Rizzano G. Cyclic behavior and modeling of a dissipative connector for cross-laminated timber panel buildings. J Earthq Eng 2014;19(1):137–71. http://dx.doi.org/10.1080/13632469.2014.948645.

[33] Jaspart JP, Weynand K. Design of joints in steel and composite structures. Ernst-Sohn; 2016, http://dx.doi.org/10.1002/9783433604762.

[34] Scotta R, Marchi L, Trutalli D, Pozza L. A dissipative connector for CLT buildings: Concept, design and testing. Materials 2016;9(3):1–17. http://dx.doi.org/10.3390/ma9030139.

[35] Marchi L, Trutalli D, Scotta R, Pozza L. Macro-element modelling of a dissipative connection for CLT structures. Structures 2020;26(April):582–600. http://dx.doi.org/10.1016/j.istruc.2020.04.044.

[36] Trutalli D, Marchi L, Scotta R, Pozza L. Capacity design of traditional and innovative ductile connections for earthquake-resistant CLT structures. Bull Earthq Eng 2019;17(4):2115–36. http://dx.doi.org/10.1007/s10518-018-00536-6.

[37] Hashemi A, Quenneville P. Large-scale testing of low damage rocking cross laminated timber (CLT) wall panels with friction dampers. Eng Struct 2020;206(January):110166. http://dx.doi.org/10.1016/j.engstruct.2020.110166.
[38] Hashemi A, Zarnani P, Quenneville P. Development of resilient seismic solutions for timber structures in New Zealand using innovative connections. Struct Eng Int 2019;1–8. http://dx.doi.org/10.1080/10168664.2019.1696660.
[39] Marchisella A, Cervio M, Muciaccia G. Seismic design and experimental investigation of a new timber hold-down connection. In: 17th world conference on earthquake engineering, 17WCEE. 2020, p. 1–12.
[40] Denton S. Eurocodes 2G overview. In: Eurocode conference. Berlin; 2023, May.
[41] ETA-20/0007. SHD and SHD-p hold-downs SHL angle-brackets. Three-dimensional nailing plate (angle brackets and hold-downs for timber-to-timber or timber-to-concrete connections). 2021.
[42] EN 10025-2. Hot rolled products of structural steels - Part 2: Technical delivery conditions forn non-alloy structural steels. 2004.
[43] EN 14080. Timber structures — Glued laminated timber and glued solid timber — Requirements. 2017.
[44] prEN 1992-1-1. Eurocode 2 - design of concerete structures - part 1-1: General rules and rules for buildings, bridges and civil engineering structures. 2023.
[45] EN 12512. Timber structures - Test methods - Joints made with punched metal plate. 2001.
[46] zur Kammer T. Three-dimensional load-bearing behaviour of multi-storey timber frame buildings (german) (Ph.d. thesis), Technischen Universität Carolo-Wilhelmina zu Braunschweig; 2006, http://dx.doi.org/10.24355/dbbs.084-200605170200-25.
[47] prEN 1995-1-1. Eurocode 5 - Design of timber structures Part 1-1: General rules and rules for buildings. 2023.
[48] prEN 1993-1-1. Eurocode 3 - Design of steel structures. Part 1-1: General rules and rules for buildings. 2023.
[49] Ringhofer A, Brandner R, Blaß HJ. Cross laminated timber (CLT): Design approaches for dowel-type fasteners and connections. Eng Struct 2018;171(May):849–61. http://dx.doi.org/10.1016/j.engstruct.2018.05.032.
[50] Blaß HJ, Uibel T. Tragfähigkeit von stiftförmigen verbindungsmitteln in brettsperrholz. Tech. rep., 2007, URL: https://publikationen.bibliothek.kit.edu/1000006318.
[51] EN 1992-4. Eurocode 2 - Design of concrete structures - Part 4: Design of fastening for use in concrete. 2018.
[52] ETA-09/0061. Friulsider injection system KEM-UP 934 for concrete. 2014.
[53] ETA-10/0423. Torque controlled expansion anchor made of galvanised steel of sizes M6, M8, M10, M12, M16, M20 and M24 for use in concrete. 2011.
[54] prEN 1998-1-1. Eurocode 8 - Design of structures for earthquake resistance - Part 1-1: General rules and seismic action. 2022.
[55] Muciaccia G. Behavior of post-installed fastening under seismic action. ACI Struct J 2017;114(1):75–86. http://dx.doi.org/10.14359/51689425.
[56] Fardis MN. Seismic design, assessment and retrofitting of concrete buildings. London: Springer; 2009, http://dx.doi.org/10.1007/978-1-4020-9842-0.
[57] Simões da Silva L, Rebelo C, Nethercot D, Marques L, Simões R, Vila Real PM. Statistical evaluation of the lateral–torsional buckling resistance of steel I-beams, Part 2: Variability of steel properties. J Constr Steel Res 2009;65(4):832–49. http://dx.doi.org/10.1016/j.jcsr.2008.07.017.
[58] ISO-IEC DTR 21141. Timber structures: Timber connections and assamblages - Definition of yield point and ductility from test data. 2017.
[59] Wald F, Sokol Z, Steenhuis M, Jaspart JP. Component method for steel column bases. Heron 2008;53(1–2):3–20, URL: https://research.tue.nl/files/2975629/Metis219760.pdf.
[60] prEN 1993-1-14. Eurocode 3 - Design of steel structures Part 1-14: Design assisted by finite element analysis. 2023.
[61] Rinaldin G, Amadio C, Fragiacomo M. A component approach for the hysteretic behavior of connections in cross-laminated wooden structures. Earthq Eng Struct Dyn 2013;44(June):657–75. http://dx.doi.org/10.1002/eqe.
[62] Shanley F. Inelastic column theory. J Aeronaut Sci 1947;14(5):261–8. http://dx.doi.org/10.2514/8.1346.
[63] Dodd LL, Restrepo JI. Model for predicting cyclic behavior of reinforcing steel. J Struct Eng 1995;121(3):433–45. http://dx.doi.org/10.1061/(asce)0733-9445(1995)121:3(433).
[64] Strand7. Using strand7/straus 7. In: Introduction to the strand/straus7 finite element analysis system. 2010, URL: www.strand7.com.
[65] Cook R, Malkus D, Plesha M. Concept and applications of finite element analysis. 4th ed.. Wiley; 2002.
[66] Möhler K, Herröder W. Obere und untere reibbeiwerte von sägerauhem fichtenholz (The range of the coefficient of friction of spruce wood rough from sawing). Holz als Roh- und Werkstoff: Eur J Wood Wood Ind 1979;37(1):27–32. http://dx.doi.org/10.1007/BF02614998.
[67] Gečys T, Bader TK, Olsson A, Kajenas S. Influence of the rope effect on the slip curve of laterally loaded, nailed and screwed timber-to-timber connections. Constr Build Mater 2019;228. http://dx.doi.org/10.1016/j.conbuildmat.2019.116702.
[68] Rugarli P. Steel connection analysis. Hoboken: Wiley; 2018, http://dx.doi.org/10.1002/9781119303510.
[69] Hunt R, Bryant A. Laterally loaded nail joints in wood. J Struct Eng (U Stat) 1990;116(1):111–24. http://dx.doi.org/10.1061/(ASCE)0733-9445(1990)116:1(111).
[70] Chui Y, Ni C, Jiang L. Finite-Element model for nailed wood joints under reversed cyclic load. ASCE J 1998;96. http://dx.doi.org/10.1061/(ASCE)0733-9445(1998)124:1(96).
[71] Resch E, Kaliske M. Numerical analysis and design of double-shear dowel-type connections of wood. Eng Struct 2012;41:234–41. http://dx.doi.org/10.1016/j.engstruct.2012.03.047.
[72] Steenhuis M, Wald F, Sokol Z, Stark J. Concrete in compression and base plate in bending. Heron 2008;53(1–2):51–67, URL: https://heronjournal.nl/53-12/3.html.
[73] Gino D, Miceli E, Castaldo P, Recupero A, Mancini G. Strain-based method for assessment of global resistance safety factors for NLNAs of reinforced concrete structures. Eng Struct 2024;304(February):117625. http://dx.doi.org/10.1016/j.engstruct.2024.117625.
[74] Payen DJ, Bathe KJ. The use of nodal point forces to improve element stresses. Comput Struct 2011;89(5–6):485–95. http://dx.doi.org/10.1016/j.compstruc.2010.12.002.
[75] Southwell RV. On the analysis of experimental observations in problems of elastic stability. Proc R Soc Lond Ser A 1932;135(828):601–16. http://dx.doi.org/10.1098/rspa.1932.0055.
[76] Priestley N, Calvi GM, Kowalsky M. Displacement-based seismic design of structures. Pavia: IUSS Press; 2007.
[77] Tremblay R. Inelastic seismic response of steel bracing members. J Constr Steel Res 2002;58(5–8):665–701. http://dx.doi.org/10.1016/S0143-974X(01)00104-3.
[78] Gioncu V, Mazzolani FM. Ductility of seismic resistant steel structures. London;NewYork: Spon Press; 2002, http://dx.doi.org/10.1201/9781482271904.
[79] Kuwamura H. Transition between fatigue and ductile fracture in steel. J Struct Eng 1997;123(7):864–70. http://dx.doi.org/10.1061/(asce)0733-9445(1997)123:7(864).
[80] ETA-11/0086. Rotho blaas WHT hold downs and angle brackets. 2015.
[81] Sartori T, Tomasi R. Experimental investigation on sheathing-to-framing connections in wood shear walls. Eng Struct 2013;56:2197–205. http://dx.doi.org/10.1016/j.engstruct.2013.08.039.